Earthquake prediction in Pakistan

Dr. L. Seeber
Dr. K. Jacob

EARTHQUAKE PREDICTION IN PAKISTAN

Dr. L. Seeber
Dr. K. Jacob
Lamont-Doherty Geological Observatory of Columbia University
Palisades, New York 10964

USGS CONTRACT NO. 14-08-0001-16749
Supported by the EARTHQUAKE HAZARDS REDUCTION PROGRAM

[Reports - OPEN FILE] NO. 80-1157

U.S. Geological Survey
OPEN FILE REPORT

FINAL TECHNICAL REPORT

Sponsored by the USGS Award No. 14-08-0001-16749

Effective 3/27/79

Expires 3/27/80

Amount $60,000

EARTHQUAKE PREDICTION IN PAKISTAN

Contractor

Lamont-Doherty Geological Observatory of Columbia University

Palisades, New York 10964

Principal Investigators

Dr. L. Seeber

Dr. K. Jacob

Government Technical Officer

Dr. Jack Evernden

ABSTRACT

The continental convergence zone of the Himalaya and the Chaman transform zone are studied primarily from local seismic network data and from teleseismic and historic intensity data. We subdivide the Himalayan thrust into a shallow dipping Detachment, the portion of the thrust between the subducting Indian shield and the sedimentary wedge, and a Basement Thrust, the portion of the thrust between subducting shield and the overriding Tethyan slab. The great Himalayan earthquakes occur on the Detachment which appears aseismic otherwise, whereas the intermediate and smaller magnitude thrust earthquakes occur along a narrow belt just down-dip of the Basement Thrust Front (BTF), the boundary between the Detachment and the Basement Thrust. Local network data and modeling of teleseismic P and S waves show that these basement thrust earthquakes range in depth between 12 and 20 km and delineate a thrust fault dipping from 20 to 30°. Downdip of this narrow seismic belt the Basement Thrust appears to be aseismic. In these characteristics continental subduction in the Himalaya resembles closely oceanic subduction zones with wide accretionary wedges as the zone that ruptured in the great 1964 Alaska earthquake.

The BTF corresponds closely with the very pronounced topographic "step" between the High and the Lesser Himalaya and with a small circle of 1700 km radius, along the central 1600 km of the Himalayan arc. Along the extremity of the arc, the BTF and topographic step deviate from the small circle but remain closely associated. At the western syntaxis the BTF and the topographic step is traced straight through the hairpin bend of the surface structures and extends beyond into the Hazara arc for at least 100 km. The Hazara arc is then part of the

Himalayan front. The very extensive Detachment under the Hazara thrust-fold belt coincides with a thick Infracambrian evaporite layer and the unusual features of this belt, including the Salt range and the syntaxis, are ascribed to weak detachment coupling. Weak vs. strong detachment coupling (e.g. salt vs. no salt) are found to be important factors in shaping other thrust-fold belts such as the Appalachians.

Seismic hazard is highest in the sedimentary zone above the Himalayan Detachment, especially in the highly populated flood plains. This hazard is easily underestimated during the aseismic interseismic periods. In Hazara the Detachment may slip aseismically. A good understanding of the tectonics and seismic potential along the Himalayan Detachment can serve as a guide to estimate the hazard along similar active structures.

Moreover, long range forecasting of the great detachment earthquakes may be possible if the configuration of the great ruptures can be deduced from the data in light of our tectonic model.

Local network data and teleseismic data from the Chaman continental transform zone indicates:

1. Recent intermediate and low magnitude earthquakes occur mostly on the faults which were probably associated with the four known major earthquakes in this area (1892, 1931, 1931, 1935) but they are concentrated near the inferred ends of these major ruptures.
2. A composite fault plane solution of activity on the 1935 Quetta earthquake fault shows left-lateral slip.
3. The Chaman fault-zone south of the 1892 break (30.3°N) is a series of subparallel left-lateral strike-slip faults which include the Quetta fault. Seismicity in this section is high, but it does not include any major event ($M \geq 7.5$) and is characterized by low stress drops. A comparison between

this section of the Chaman fault system and the San Andreas fault system south of the big bend is suggested.

4. A recent abrupt increase in seismicity along the Chaman fault south of the 1892 break (30.3°N) warrants careful consideration as a premonitory signal.

5. The maximum hypocentral depths from network data range from 15 km west of Quetta to 50 km near the axis of the Sibi reentrant east of Quetta suggesting a similar thickening of the crust from west to east.

RESULTS

The main purpose of the subject contract work is to improve the understanding of the earthquake hazard associated with the active continental collision front of the Himalaya. Our contributions stem from two distinct lines of research: Resolution of the details of the active tectonics at the northwestern end of the Himalayan arc from seismic network data, and synthesis of the available data about the entire Himalaya into a model for the active tectonics of this structure. We feel that an acceptable model for the active tectonics is the basic prerequisite for any conditions regarding seismic hazard and for earthquake prediction.

TECTONIC MODEL FOR THE HIMALAYA

The details of the seismicity in the Himalaya and the essential features of other available surface and subsurface data fit into a simple scheme of the active tectonics (Figure 4). In this scheme there are three main elements: a subducting basement slab, the Indian shield; an overriding basement slab, the Tethyan slab; and a sedimentary wedge stretching above the subduction zone and decoupled from both basement slabs. Accordingly, there are a shield zone where the subducting

basement is still at the surface; a Tethyan zone where the subducted slab below and the passive slab above are layered into a very thick crust; and a sedimentary zone, the area covered by the sedimentary wedge. Thus, the sedimentary zone includes the foredeep, the Sub-Himalaya and the Lesser Himalaya; while the Tethyan zone includes the High Himalaya, the Tethys Himalaya and an unspecified part of the Tibetan Plateau.

The fundamental active thrust fault of the Himalaya is located on the upper surface of the subducting slab. The Detachment is the portion of this fault between the subducting slab and the sedimentary wedge. The Basement Thrust is the portion of this fault between the interacting slabs. The Basement Thrust Front (BTF) marks the line separating the very shallow-dipping Detachment from the steeper-dipping Basement Thrust. The Basement Thrust is subdivided into a narrow seismically active portion adjacent to the BTF, and into an aseismic but presumably still active portion of unknown extent further down-dip.

The narrow belt of thrust earthquakes which define the BTF (Figures 6 and 8) is associated with the very pronounced topographic step between the Lesser and the High Himalaya (Figure 8). These two features are continuously correlated over the entire 2,500 km long Himalayan arc. The central 1,700 km of this arc is found to fit closely a small circle. This remarkable fit suggests that the arcuate slope is required by the ongoing Himalayan tectonics, and confirms that the BTF is its fundamental feature. The radius of the small circle (1,700 km) predicts a 30° dip at the BTF in order to minimize the stretching of the spherical slab at the downward bend. This dip angle is within the scatter of the dip angles obtained from fault plane solutions (Molnar et al., 1977).

In Hazara the location of the BTF is well known from the seismic network data (Figure 5, IKSZ). Here the BTF is located at the updip end of the IKSZ thrust at a depth of about 12 km and the dip of the seismically active thrust zone is about

30° (Seeber and Armbruster, 1979). In the rest of the Himalaya the location of the BTF is only known to the accuracy of the teleseismic hypocentral determinations. Teleseismic hypocenters are relatively inaccurate, particularly in the depth coordinate (we don't expect a systematic bias due to lateral inhomogeneities because we don't find a systematic bias between hypocenters determined from teleseismic data and local network data). In an ongoing project we analyzed 3 of the larger BTF earthquakes plotted in Figure 6 with a P and S wave modeling technique (Helmberger and Burdick, 1979) and more reliable fault plane solutions and depths were determined. The revised depths range from 15 to 20 km (15 to 50 km in the NOAA data, see Figure 6) and the fault plane solutions are consistent with a thrust plane and slip vector dipping normal to the strike of the BTF at the hypocenter.

The scattered seismicity in the Tethyan zone, north of the thrust earthquake belt, is associated mostly with normal faulting and is consistent with east-west extension (Ni and York, 1978; Molnar and Tapponnier, 1978). None of the available solutions for this area are consistent with slip on a shallow-dipping fault. On the other hand, the great Himalayan earthquakes (1897, 1905, 1934) occur south of the BTF, in the sedimentary zone, and are Detachment slip events. None of the 3 well documented great Himalayan earthquakes are associated with rupture on the Main Boundary Thrust (MBT). Geodetic data for the area of the 1905 event (Middlemiss, 1910; Chugh, 1974) is consistent with a shallow dipping thrust below the MBT and part of the foredeep. In the interseismic periods (between the great events) thrust earthquakes are concentrated at the BTF and the Detachment appears to be aseismic. This observation is crucial for correctly estimating the seismic hazard along the Himalayan arc.

At the northwestern terminus of the Himalayan arc, in Hazara, locally monitored seismicity and microseismicity in the sedimentary zone south of the BTF

is primarily, either within the subducting basement slab, or in the sedimentary wedge (Figure 5). The seismicity in the basement is mostly on tear faults and on transcurrent faults, respectively transverse and parallel to the BTF. Within the sedimentary wedge the seismicity is concentrated in a relatively small and sharply defined volume. Normal faulting in the subducting slab due to the downward bending is deduced from one fault plane solution in the foredeep of the central Himalaya but is not observed in Hazara. However, scattered seismicity deeply reaching in the subducting basement slab near the BTF can be a consequence of the bending (Armbruster et al., 1978; Seeber and Jacob, 1977; Seeber and Armbruster, 1979).

The Detachment in Hazara is relatively aseismic, however some earthquakes are associated with this fault. While the seismicity within the basement and the sedimentary wedge in Hazara can be representative of the rest of the Himalayan arc, the mode of slip on the Detachment in Hazara is probably anomalous since in this area the Detachment is extensively associated with a thick evaporite layer which is not found in the central Himalaya (oil exploration data; Mathur and Kohli, 1964).

Even a thin and weak sediment layer can transfer sufficient force to propagate the deformation forward in a thrust and fold belt if the sediment layer is very weakly coupled to the basement (Chapple, 1978). Thus a wide belt of deformation can be expected where the detachment occurs at a weak salt layer. This suggests that the shaping of the western terminus of the Himalayan deformational front into the Hazara arc and the location of the Hazara-Kashmir syntaxis reflects the distribution of very weak coupling at the detachment associated with the Infracambrian salt layer (Seeber et al., 1980). In this hypothesis the syntaxis and the related Jhelum reentrant mark the boundary between strong basement-sediment coupling with presumably no salt on the east side, and weak coupling with salt on the west side (Figures 9b and 10).

Earthquake Hazard in the Himalayan in Both Space and Time

The model which we have developed describes the active tectonic processes of the Himalaya and provides a framework within which seismic hazard can be better estimated in space, and suggest lines of research which can lead to a reliable space-time hazard evaluation, i.e. to long term forecasting of great earthquakes. Although locally destructive earthquakes can occur near the Basement Thrust front (BTF), along the belt of intermediate magnitude thrust earthquakes, the greatest hazard is from the much larger Detachment earthquakes that rupture south of this belt. In the Hazara area the Detachment is associated with a thick layer of salt and the lack of seismicity on the Detachment may be associated with aseismic slip on the salt. The hazard in this area may be low but in the remainder of the Himalayan arc, lack of seismicity on the Detachment is associated with strain accumulation between great earthquakes. These events can be expected to effect large areas of the Lower Himalaya, and the densely populated Indo-Gangetic plain as they have in the past.

In the last two centuries great Himalayan earthquakes have occurred at an average rate of about one every 30 years. If we can deduce the rupture areas from the available data (surface effects and instrumental) and if we can assume that the rate of great earthquake occurrence in the last 100 years is representative of the long term study state seismicity, then we can obtain an estimate of the repeat time and we can produce long term forecast for the great earthquakes. We are now studying the intensity data for the 1897, 1905, 1934 and 1950 earthquakes, and the implication this data has regarding the respective areas of rupture.

APPALACHIANS, HIMALAYAS AND GULF OF ALASKA COMPARED

The fossil continental collision zone of the southern Appalachians and the active oceanic subduction zone of Alaska are compared to the continental collision and subduction zone of the Himalaya in Figure 11. The main features of the three structures are remarkably similar. In all three cases there is a sedimentary wedge (usually referred to as an accretionary prism in the case of oceanic subduction) detached from the underlying basement. This detachment merges down-dip into a basement thrust. The basement block forming the hanging wall of this thrust provides the support on the hinterland side of the wedge. In the southern Appalachian section there is a suggestion that the BTF is at the base of the Kings Mt. crystalline belt (R.D. Hatcher, personal communication). An alternative interpretation of the subsurface data (Cook et al., 1979) puts the basement thrust at an undetermined distance further southeast.

In the Himalaya the MBT is the boundary between terrigenous and pre-collisional shelf sediments. Thus most of this wedge is composed of these terrigenous sediments. Instead, in the southern Appalachians the terrigenous sediments are a relatively minor component of the wedge. (Note that in Figure 11 the "younger sediments" in the Himalayan section are all terrigenous while in the Appalachian section only a portion of the "younger sediments" are terrigenous). As continental subduction continues, the ratio between terrigenous and precollisional sediments in the central Himalayan wedge increases because erosion effects primarily the precollisional sediments of the Lesser Himalaya and the eroded material is replaced exclusively by terrigenous sediments (assuming that the total volume of the wedge remains constant). This suggests that continental subduction in the Appalachians, if it followed continental collision at all, may have been shorter lived than in the Himalaya.

Probably most of the Himalayan Detachment occurs at the boundary between the terrigenous sediments and the crystalline basement. In the southern Appalachians the Detachment is believed to coincide mostly with a layer of low shear-strength, the Rome shale (Hatcher, 1978). The large width of the Appalachian fold and thrust belt may be symptomatic of the effectiveness of the decoupling layer. In fact, the dimensions and structure of the Valley and Ridge province are similar to those of the Potwar in the outer wedge of Hazara (Figures 5 and 10b). Here the wedge is well decoupled from the basement by the evaporite layer and contains a large proportion of precollisional sediments.

In the Gulf of Alaska oceanic lithosphere of the Pacific plate subducts below the continental lithosphere of the North American plate. Although the accretionary wedge is unusually wide, probably because of the large input of sediments into the Gulf of Alaska, the Alaska subduction zone in Figure 11 is a rather typical example of this type of structure. The mode of slip along the main fault is remarkably similar in the Alaskan and Himalayan subduction structures. In each, three portions of the fault can be distinguished down-dip from the trench: (1) a Detachment, (2) a seismically active Basement Thrust, and (3) an aseismic portion of this Basement Thrust. In both cases the Detachment characteristically slips by great earthquakes. During these events the extent of rupture and the displacement are typically measured in hundreds of kilometers and tens of meters, respectively. It is a hypothesis of ours (Seeber et al., 1980) that the Detachment is the lower boundary of the sedimentary wedge and is delimited by the ruptures of great earthquakes (Figure 11). The interseismic periods on the Detachment are typically 40 years to a few hundred years at oceanic subduction zones. In the Himalaya they are undetermined, but probably at least 100-200 years. During these periods the Detachment appears to be almost or completely aseismic (Figure 11 for Alaska, Figure 6 for the Himalaya).

At the down-dip end of the Detachment the Basement Thrust Front (BTF, Figure 4) marks the up-dip end of the Basement Thrust. This portion of the thrust is characterized by intense seismicity, which, in contrast with the seismicity on the detachment, is relatively continuous. The seismicity is characterized by moderate magnitude and smaller events (Davies and House, 1979). It is this seismicity along the Basement Thrust that forms the narrow earthquake belt of the Himalaya (Figures 6 and 8). In the oceanic subduction zone this seismicity also forms a narrow belt at the shallow end of the Benioff zone that otherwise consists mostly of hypocenters within the sinking slab (Isacks and Barazangi, 1977).

The sedimentary wedge is decoupled from both plates interacting at the subduction zone. The detachment is the active boundary between the wedge and the subducting plate. The boundary with the other plate at the back of the wedge is not as clearly defined. However, this boundary should also be active since it divides a wedge of weak sediments that deform viscously from a slab of strong crystalline rocks that behaves rigidly (cf. Figures 4 and 10). In the Himalaya this boundary is at or near the MCT (Figure 4). Shallow seismicity above the BTF, similar to the seismicity near Cook Inlet in the Gulf of Alaska (Figure 11), is found in many other closely monitored subduction zones (Davies and House, 1979; Isacks and Barazangi, 1977; Engdahl, 1977; Uyeda, 1977). In our interpretation the aseismic front (Yoshii, 1975) is the forward boundary of the rigid overriding plate. Thus, the great detachment earthquakes are not true interplate earthquakes, since the sedimentary wedge above the detachment is not rigidly connected with either of the converging plates. Rather it is the belt of moderate-magnitude thrust-earthquakes that marks the contact between the two plates and is the most fundamental seismic expression of the plate boundary.

Down-dip from the seismically active portion of the Basement Thrust this feature usually becomes steeper in oceanic subduction zones, but presumably

becomes shallower-dipping, bending back to a quasi-horizontal fault, in the Himalayan subduction zone. However, the slip on both these boundaries becomes similarly aseismic (see earlier discussion for the Himalayan case, Isacks and Barazangi, 1977; Engdahl and Scholz, 1977; discuss the oceanic subduction case). In both continental and oceanic subduction the transition between seismic and aseismic slip may be ascribed to shear heating and/or interaction of water from the underthrusting slab with the hot rocks at the base of the overriding slab.

INTERPRETATION OF LANDSAT IMAGERY*

[*This work is carried out by L. Seeber and by Vivien Gornitz at the Goddard Institute of Space Studies, New York. This work by V. Gornitz was not financed by the subject contract.]

In the Hazara arc region of northern Pakistan, where a seismic network has been operating since 1973, interpretation of seismic data has found that a detachment separates surface structures from the deeper basement thrust of the Himalayan front (Figure 10b). The Basement Thrust, as indicated by the Indus Kohistan Seismic Zone (IKSZ), is marked by a pronounced topographic break (Figure 8). In this study, other surface expressions of the basement tectonics have been sought, by analysis of lineaments and stream drainage patterns from LANDSAT satellite imagery.

Lineaments have been compared directly with seismicity maps from the Tarbela seismic network (Figure 12). Lineament data have been summarized on standard rose diagrams, and a fracture-intersection density map has been constructed for a strip along the Indus Valley. Longitudinal stream profiles were drawn from ONC topographic maps. The spatial distribution of knickpoints, or sharp changes in topographic gradient, has been examined (Figure 13). We conclude:

1. Landsat imagery shows a N-S trending set of lineaments along the Indus River and NW-trending lineaments roughly aligned with the IKSZ. Fractures are concentrated at the intersection of these two lineament trends, less than 20 km south of IKSZ and along the Indus River 25 km north of Tarbela. The NW-trending belt is the only LANDSAT lineament obviously associated with current seismic activity, occurring in the lower crust below the detachment. The lineaments along the river can be associated with the Indus anticline/horst and related reentrant (Calkins et al., 1975) which is recognized from Tarbela dam to Besham Quila (Figure 13) (Seeber, work in progress). No seismic zone is associated with this feature.

2. Longitudinal profiles of the Indus tributaries show knickpoints in the area between Pattan and Beshem Qila, slightly north of the IKSZ in an area of high seismicity. Two streams draining south of the IKSZ show no knickpoints. A tectonic origin for the knickpoints is suggested by the proximity to the IKSZ. Knickpoints only occur upstream (NE) of the IKSZ, indicating that the NE side is uplifting with respect to the SW side of the IKSZ.

3. Hypsometric curves of Indus river tributaries near the IKSZ indicate that while all of the basins are "mature", the Siran basin, the only one of these basins draining south of the IKSZ, is "overmature", i.e. more strongly eroded. This difference cannot be explained by differential erosion since the hard rocks along the rivers examined, including the Siran river (granites, quartzites; Calkins et al., 1975) seem equally resistent to erosion. Thus, the hypsometric curves may indicate a relaitvely early age of uplift for the Siran basin. Alternatively a differential rate of uplift within the Siran basin, higher toward the source area at the IKSZ and lower downstream, southwest of the IKSZ, can also give a basin a more "eroded" profile. This latter explanation is consistent with the differential uplift at the IKSZ suggested by the knickpoints (see above).

4. Landsat imagery provides examples of disrupted drainage and river capture, which can be related to recent tectonism. From Landsat, the Peshawar Basin appears bounded on the north by NW and NE trending faults. The seismic data indicates a similar fault pattern where the movement is consistent with north-south compression (Armbruster et al., 1978). Several of the Landsat lineaments correspond directly with seismic lineaments of that study.

5. In general, linears obtained from satellite imagery and river profiles are found to be diagnostic of basement faults active below a decollement and with no direct surface expression. These basement faults do not appear at the surface as a single fault with a large displacement. Instead they manifest themselves as relatively wide zones with a large number of subparallel faults. The displacement at the surface may be taken up by these faults and by folding.

THE QUETTA FAULT AND THE CHAMAN TRANSFORM SYSTEM

According to the theory of plate tectonics, the Indian plate is moving northward with respect to its adjacent stable block, the Eurasian plate (Molnar and Tapponnier, 1975). The rate of convergence is approximately 3.5 cm/yr near the longitude of Quetta (Minster and Jordan, 1978). The Chaman fault (Figure 1) is usually considered the active boundary between the Indian plate and the micro-plates Iran and Afghanistan which may be only loosely attached to Eurasia (Powell, 1979). Plate tectonics requires left-lateral strike-slip on this boundary. This left-lateral motion may not be fully taken up by the Chaman fault, but it may occur on a number of subparallel faults within a wide zone of deformation.

The Quetta area has been the location of a number of large destructive earthquakes (Figures 2 and 14). The general north-northeast trend of the elongated mezoseismal zones observed in 1892, 1931 and 1935 is consistent with the observed

geologic structure and the direction of motion of India with respect to Eurasia (Figures 2 and 14). However, the transverse trend of the mezoseismal zone of the 1909 event, the aftershock zone of the 1931 event and the ongoing seismic activity of the Quetta transverse ranges attest to the complexity of the active tectonic patterns of this area. From June to December 1978 a network of five telemetered seismic stations was operated in the Quetta area for the study of tectonics and earthquake prediction in a cooperative effort between the Lamont-Doherty Geological Observatory, New York, and the Geological Survey of Pakistan, Quetta. Within the area in which earthquakes were located by the Quetta seismic network there have been three historic earthquakes with an intensity (Modified Mercalli scale) of eight and greater. In addition a number of earthquakes which occurred prior to installation of the Quetta seismic network were large enough to be located by seismic instruments operating around the world (teleseismic epicenters; Figures 3 and 14).

Microearthquake Data:

Chaman Fault. This fault is the most active seismic zone observed by the Quetta network. About half of all the microearthquake epicenters in Figure 14 occur along the Chaman fault, within the possible error in location. Considering the distance of this fracture from the network ($\sim$70 km), this seismic source must be at least an order of magnitude more active than the area within the seismic network. Most of these microearthquakes fall on the same segment of the Chaman fault presumably associated with the three recent teleseismically located events, the 3 October 1975, magnitude M_S 6.4 and 6.7 Spin Tezha earthquakes, and the 16 March 1978, magnitude M_S 5.9 Nushki earthquake (Figure 14). It is possible that the microearthquakes occurring on the Chaman fault 36 and 7 months, respec-

tively, after these moderate size earthquakes are part of a prolonged and complex aftershock sequence.

Quetta Fault. The northern portion of this fault, which by definition ruptured in the 1935 Quetta earthquake, is well covered by the Quetta network. A number of hypocenters aligned with the Chiltan ridge and located northwest of Quetta are probably associated with this fault (Figure 15). Most of these hypocenters cluster near the northern end of the 1935 mezoseismal zone and occur to the north of all the located 1935 aftershocks (Figure 14). It is possible that most of the current seismicity on the Quetta fault occurs beyond but near the north end of the 1935 rupture (Figure 17). Only four epicenters correlate with the central portion of the fault which ruptured in 1935.

The hypocentral locations, focal mechanism and mapped faults (Jones, 1961) are all consistent with a fault or fault-zone striking north-northeast and steeply dipping to the west-northwest. The apparently complex distribution of hypocenters on the Quetta fault-zone in Figure 16 may be ascribed to activity on more than one parallel fault and/or to the bending of these faults north of the Quetta valley. The composite focal mechanism of these events (Figures 15 and 16) indicates the northern portion of the Quetta fault is presently undergoing left-lateral motion.

Chaman vs. San Andreas Transform Boundaries Compared

Historic, teleseismic and network data examined together indicate that since 1975 the pattern of seismicity in the Quetta area is characterized by unusually high activity on the Chaman fault west of Quetta.

A 3/4 meter displacement was observed on the Chaman fault near the town of Chaman after the 1892 event (Griesbach, 1893). In contrast to reports indicating repeated offsets on the Chaman fault occurring in the 19th century

(McMahon, 1897), no offsets are reported for the period between 1892 and 1975 (Figure 2) although two railways cross the fault (at 30.8°N and 29.4°N) and the area has been occupied by military garrisons.

A pattern similar to the distribution of reported intensities (Figure 2) is obtained from the teleseismic data prior to 1975 (Figure 3). The seismicity along the fold belt east and south of Quetta is generally high, but no epicenters occur along the Chaman fault south of latitude 31°N. However, most of the seismicity detected since 1975 in the area of Figure 14 is concentrated along the Chaman fault south of the southern limit of the 1892 mezoseismal area at about 30.3°N (Heuckroth and Karim, 1970). This recent seismicity includes three teleseismic epicenters, the Spin Tezha 1975 (M_S = 6.4 and 6.7) and the Nushki 1975 (M_S = 5.9) earthquakes, and most of the microearthquakes detected by the Quetta network.

Thus, there has been a recent increase of seismicity on the Chaman fault south of the 1892 event. However, the possibility of another such burst of activity on this section of the Chaman fault after 1892 and before 1963, when the teleseismic detection level in this area was lowered to about magnitude M_b = 4.8 (Seeber et al., 1979), cannot be ruled out. The seismicity along the Quetta fault after the 1935 event is also concentrated at the extremities of the rupture zone as determined from the mezoseismal area. Four out of five of the teleseismic epicenters that can be related with the Quetta fault occur within 30 km of either of the extremities of the 150 km long presumed rupture (Figures 14 and 17). Given the uncertainty of the locations these earthquakes may have occurred on the Quetta fault very near the extremities of the fracture. The February 18, 1955 (M 6.2) event is particularly significant because a mile-long fissure was observed after this event along the northern extension of the Chiltan fault in the Quetta valley north of Quetta, at the presumed northern extremity of the 1935 rupture. The network data for the Quetta fault (Figures 14 and 15) confirm the pattern of

seismicity indicated by the teleseismic data. Microearthquake hypocenters cluster in a 30 km segment of the Quetta fault at the northern extremity of the 1935 rupture.

Thus, the general pattern of seismicity in the Quetta area is one of large events and aftershock sequences. During the interseismic periods the segments of the faults that ruptured at the large events are almost aseismic and the seismicity is concentrated at the extremities of these segments. Such a pattern has been observed in California along the San Andreas fault system (Allen, 1975). The 150 km long segment of the San Andreas fault between the northern end of the 1857 and the southern end of the 1906 breaks never ruptured in a major event during historic times. A detailed examination of surface displacement and geodetic data in this segment of the fault (Brown and Wallace, 1968; Savage and Burford, 1973) indicate that the slip in the last 60 years has been rather continuous and uniform at about 3.2 cm/year, a rate which probably corresponds to the long term rate of slip. Thus, strain energy for a large event in this segment of the San Andreas fault is not accumulating. In the same segment, the seismicity is characterized by small and intermediate earthquakes ($M < 6.5$; see below) with relatively short recurrence times (an earthquake which is "intermediate" may still be destructive locally). On the other hand, in the segment of the San Andreas fault that ruptured in 1857, major earthquakes have occurred systematically over the past 14 centuries at an average rate of 1 earthquake every 160 years (Sieh, 1978) but few small earthquakes are occurring there now. Thus, the San Andreas fault is characterized by distinct portions with contrasting and stable patterns of behavior.

Microearthquakes on the Chaman fault recorded by the Quetta network are to far from the nearest seismic station for accurate determination of depth. The three recent teleseismically recorded events on the Chaman fault have been analyzed using body wave modeling techniques (Helmberger and Burdick, 1979) and

depth phases have been identified (in preparation). These preliminary results indicate that the three events occurred at depths of 6, 10 and 12 kilometers, within the depth range of activity on the San Andreas fault.

The San Andreas fault system in California and the Alpine fault system in New Zealand exhibit change in strike or bends such that the angle between the regional slip-vector and the strike of the master-fault varies along the fault system. Scholz (1977) compares the portion of the San Andreas fault that ruptured in 1857, known as the "big bend", with the central portion of the Alpine fault of New Zealand adjacent to the southern Alps (Figure 18). This section of the Alpine fault has not ruptured in historic time (150 years), it is not associated with intermediate or small earthquakes, it is not creeping, and it is expected to rupture in a major event, similar to the 1857 event. (Following Scholz, the magnitude in a major earthquake is $M > 7.5$, in a large earthquake $7.5 \geq M \geq 6.5$, in a moderate or small earthquake $M < 6.5$; with this definition the Quetta 1935 $M = 7.5$, is classified as a large but not major earthquake).

It is here suggested that the segment of the Chaman fault between 30°N and 33°N that includes the 1892 rupture (only the southern limit of this rupture is approximately known) fits in the same category as the segments of the San Andreas and Alpine faults mentioned above, i.e. strain relief by rare but major events.

In all these three segments the fault zone is rather narrow and it may rupture only in major earthquakes. Scholz ascribes this behavior to the relatively large angle between the slip-vector and the strike of the fault which would, in all three cases, tend to increase the normal component of stress across the fault, and hence the frictional strength. In each of the regions in Figure 18, south of the "bend" the strike of the fault system is nearly parallel to the regional slip. In these areas the fault zone widens and slip appears to be taken up by a number of subparallel faults. Furthermore, in these same sections of the fault-zones major earthquakes no not

occur, but large to small earthquakes occur frequently and, together with possible creep-zones, probably account for the total long-term slip-rate across the fault zones (see Figure 3). Data presented in this paper indicate that the Quetta 1935 event ruptured a fault subparallel to the Chaman fault and accounted for a portion of the left-lateral strike-slip taken up by this fault system.

Lawrence and Yeats (1979) have investigated the portions of the Chaman fault in Pakistan. They contrast the "long, straight active trace" of the fault in the area of the 1892 event with the "short traces, multiple en echelon traces and local absence of active traces" observed to the south, in the Nushki area. From a comparison of the contrasting surface features along the 1906 break and the "creeping" segment of the San Andreas fault with the similarly contrasting features along the 1892 segment and the Nushki segment of the Chaman fault, they suggest a pattern of major earthquakes versus creep and small earthquakes in these two segments of the Chaman fault, respectively.

The surface-wave to body-wave magnitude radio, M_s/M_b, for the three recent earthquakes in the area of Figure 13, the Spin Tezha 1975, the Nushki 1978, and the Kolpur 1977 events, are 6.4/5.7, 6.7/5.8, 5.9/5.3, and 5.5/5.1, respectively (Epicenter Determination Report, U.S.G.S.). The unusually high ratios for the three earthquakes on the Chaman fault suggest low stress-drops for these earthquakes (Archambeau, 1978). Similarly the stress-drops for earthquakes along the San Andreas fault are low and generally lower than for other earthquakes in Southern California (Thatcher and Hanks, 1973). Since the recent instrumental seismicity associated with both the San Andreas and the Chaman faults occurs along segments of these faults between major ruptures, the low stress-drops may characterize these segments only, and not necessarily the rest of the fault where major earthquakes occur.

REFERENCES

Allen, C.R. (1975). Geological criteria for evaluating seismicity, Geol. Soc. Amer. Bull., 86, 1041-1057.

Archambeau, L. (1978). Estimation of non-hydrostatic stress in the earth by seismic methods: Lithospheric stress levels along Pacific and Nazca plate subduction zones, Proceedings of Conference VI Methodology for identifying seismic gaps and soon to break gaps, U.S.G.S. Open-File Report 78-943.

Armbruster, J., L. Seeber, and K.H. Jacob (1978). The northwestern termination of the Himalayan mountain front: Active tectonics from microearthquakes, Jour. Geophys. Res., 83 (B1), 269-282.

Armbruster, J., L. Seeber, R. Quittmeyer, and A. Farah (1980). Seismic network data from Quetta, Pakistan: The Chaman fault and the fault related to the 30 May 1935 earthquake, in Proc. Geodynamic Conf., Peshawar, November 1979.

Brown, R.D., and R.E. Wallace (1968). Current and historic fault movement along the San Andreas fault between Paicines and Camp Dix, California, Proceedings of the Conference on Geologic Problems of the San Andreas Fault System, Stanford Univ. Publ. Univ. Ser. Geol. Sci., 11, 22-41.

Calkins, J.A., T.W. Offield, S.K.M. Abdullah, and S.T. Ali (1975). Geology of the southern Himalaya in Hazara, Pakistan and adjacent areas, U.S. Geol. Surv. Prof. Paper 716-C, Washington.

Chapple, W.M. (1978). Mechanics of thin-skinned fold-and-thrust belts, Geol. Soc. of Amer. Bull., 89, 1189-1198.

Chugh, R.S. (1974). Study of recent crustal movements in India and future programs, paper presented at the International Symposium on Recent Crustal Movements, Zurich.

Cook, F.A., D.S. Albaugh, L.D. Brown, S. Kaufman, J.E. Oliver, and R.D. Hatcher, Jr., (1979). Thin-skinned tectonics in the crystalline southern Appalachians: COCORP seismic-reflection profiling of the Blue Ridge and Piedmont, Geology, 7, 563-567.

Davies, J.N., and L. House (1979). Aleutian subduction zone seismicity, volcano-trench separation and their relation to great thrust-type earthquakes, Jour. Geophys. Res., 84, 4583-4591.

Engdahl, E.R. (1977). Seismicity and plate subduction in the central Aleutians, in Island Arcs, Deep Sea Trenches and Back-Arc Basins, Maurice Ewing Ser., 1, edited by M. Talwani and W.C. Pitmann III, 259-272, AGU, Washington, D.C.

Engdahl, E.R., and C.H. Scholz (1977). A double Benioff zone beneath the central Aleutians: An unbending of the lithosphere, Geophys. Res. Lett., 4, 473-476.

Gansser, A. (1964). Geology of the Himalayas, Inter-Science Publishers, John Wiley and Sons, London.

Griesbach, C.L. (1893). Notes on the earthquake in Baluschistan on the 20th December 1892, Rec. Geol. Sur. India, 26, n. 1, 47-61.

Hatcher, R.D., Jr. (1978). Tectonics of the western Piedmont and Blue Ridge, Southern Appalachians: Review and Speculation, Amer. Jour. Sci., 278, 276-304.

Helmberger, D.V. and L.R. Burdick (1979). Synthetic Seismograms, Ann. Rev. Earth Planet. Sci., 7, 417.

Heron, A.M. (1911). The Baluchistan earthquake of the 21st October 1909, Rec. Geol. Sur. India, 41, part 1, 22-35.

Heuckroth, L.E., and R.A. Karim (1970). Earthquake history, seismicity, and tectonics of the regions of Afghanistan, Kabul University, 102 p.

Isacks, B.L., and M. Barazangi (1977). Geometry of Benioff zones: Lateral segmentation and downwards ending of the subducted lithosphere, in Islands Arcs, Deep Sea Trenches and Back-Arc Basins, Maurice Ewing Ser., 1, edited by M. Talwani and W.C. Pitmann III, AGU, Washington, D.C.

Jones, A.G. (ed.) (1961). Reconnaissance geology of part of West Pakistan: A Columbo Plan cooperative Project, Government of Canada, Toronto, 550 p.

Kazmi, A.H. (1979). Active fault systems in Pakistan, in Geodynamics of Pakistan, A. Farah and K. DeJong (eds.), Spec. Publ., GSP, Quetta.

Lahr, J.C., R.A. Page, and J.A. Thomas (1974). Catalog of earthquakes in South Central Alaska, April-June 1972, U.S. Geol. Surv. Open-File Report.

Lawrence, R.D., and R.S. Yeats (1979). Geological reconnaissance of the Chaman fault in Pakistan, in Geodynamics of Pakistan,, A. Farah and K. DeJong (eds.), Spec. Publ., GSP, Quetta.

Mathur, L.P., and G. Kohli (1964). Exploration and development for oil in India, World Petroleum Congress, 6th, Frankfurt an Main, Pr. Sec. 1, 633-658.

McMahon, A.H. (1897). The southern borderlands of Afghanistan, The Geographical Jour., 9, no. 4, 393-415.

Middlemiss, C.S. (1910). The Kangra earthquake of 4th April 1905, Mem. Geol. Sur. India, 38, 1-409.

Minster, J.G., and T.H. Jordan (1978). Present-day plate motions, Jour. Geophys. Res., 83, 5331.

Molnar, P., and P. Tapponnier (1975). Cenozoic tectonics of Asia: Effects of a continental collision, Science, 189, 419-426.

Molnar, P., W.P. Chen, T.J. Fitch, P. Tapponnier, W.E.K. Warsi, and F-T Wu (1977). Structure and tectonics of the Himalaya: A brief summary of geophysical observations, Editions de C.N.R.S., 268, 269-294.

Molnar, P., and P. Tapponnier (1978). Active tectonics of Tibet, Jour. Geophys. Res., 83, 5381-5375.

Ni, J., and J.E. York (1978). Late Cenozoic extensional tectonics of the Tibetan Plateau, Jour. Geophys. Res., 83, 5377-5384.

Plafker, G. (1965). Tectonic deformation associated with the 1964 Alaska earthquake, Science, 148, 1675.

Powell, C.McA. (1979). A speculative tectonic history of Pakistan and surroundings: some constraints from the Indian Ocean, in Geodynamics of Pakistan, p. 5, edited by A. Farah and K. DeJong, Geol. Surv. Pakistan, Quetta.

Quittmeyer, R.C., and K.H. Jacob (1979). Historical and modern seismicity in Pakistan, Afghanistan, Northwest India, and Southeast Iran, Bull. Seismol. Soc. Amer., June 1979.

Quittmeyer, R.C., A. Farah, and K.H. Jacob (1979). The seismicity of Pakistan and its relation to surface faults, in Geodynamics of Pakistan, A. Farah and K. DeJong (eds.), Spec. Publ., GSP, Quetta.

Savage, J.C., and R.O. Burford (1973). Geodetic determination of relative plate motions in Central California, Jour. Geophys. Res., 78, 832-845.

Scholz, C.H. (1977). Transform fault systems of California and New Zealand: Similarities in their tectonic and seismic styles, Jour. Geol. Soc., 133, 215-229.

Seeber, L., and K.H. Jacob (1977). Microearthquake survey of northern Pakistan: Preliminary results and tectonic implications, in Proc. C.N.R.S. Coloquium on the Geology and Ecology of the Himalayas, Paris, 347-360.

Seeber, L., J. Armbruster, and S. Farhatulla (1979). Seismic hazard at the Tarbela dam site and surrounding region from a model of the active tectonics, preprint.

Seeber, L., and J. Armbruster (1979). Seismicity of the Hazara arc in northern Pakistan: Decollement vs. basement faulting, in Geodynamics of Pakistan,

p. 131-142, edited by A. Farah and K. DeJong, Geol. Survey Pakistan, Quetta.

Seeber, L., J. Armbruster, and R. Quittmeyer (1980). Seismicity and continental subduction in the Himalayan arc, Inter-Union Commission on Geodynamics, Working Group 6 Volume.

Sieh, K.E. (1978). Prehistoric large earthquakes produced by slip on the San Andreas fault at Pallett Creek, California, Jour. Geophys. Res., 83, 3907.

Thatcher, W., and T.C. Hanks (1973). Source parameters of southern California earthquakes, Jour. Geophys. Res., 78, 8547-8576.

Uyeda, S. (1977). Some basic problems in the trench-arc back-arc system, in Island Arcs, Deep Sea Trenches and Back-Arc Basins, Maurice Ewing Ser., 1, edited by M. Talwani and W.C. Pitmann III, AGU, Washington, D.C.

Wadia, D.N. (1931). The syntaxis of the northwest Himalaya - its rocks, tectonics, and orogeny, India Geol. Surv. Record, 65, part 2, 189.

West, W.D. (1934). The Baluchistan earthquakes of August 25th and 27th, 1931, Mem. Geol. Sur. India, 67, part 1, 1-82.

West, W.D. (1935). Preliminary geological report on the Baluchistan (Quetta) earthquake of May 31st, 1935, Rec. Geol. Sur. India, 69, part 2, 203-240.

Yoshii, T. (1975). Proposal of the "Aseismic Front", Zishin, 20, 365-367.

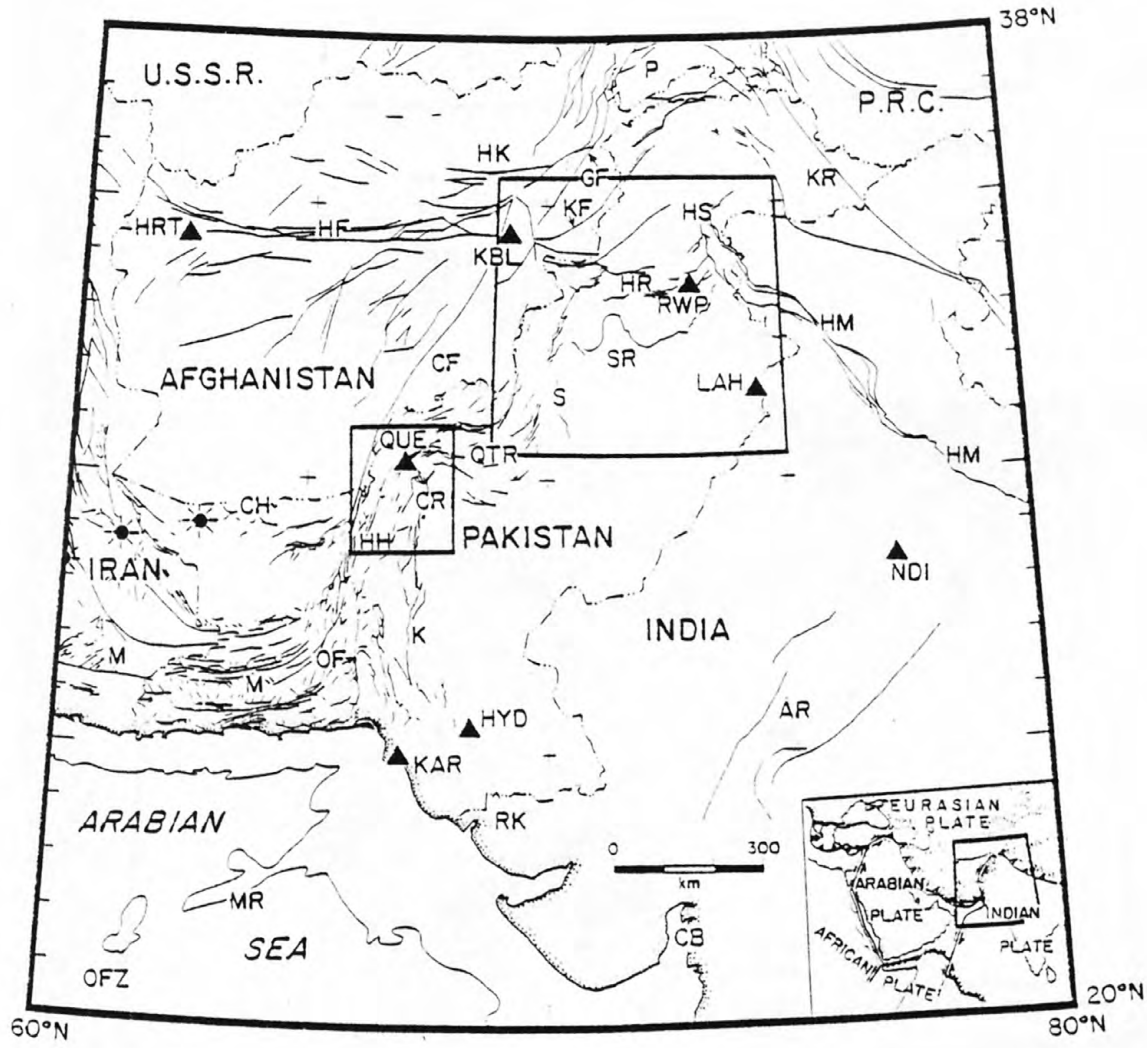

Figure 1. Index map of the northwestern boundary of the Indian subcontinent (from Quittmeyer and Jacob, 1979). Mapped surface faults are shown. The areas covered by the networks established by L-DGO are boxed in. The Tarbela and Chashma networks are in the larger box. The Quetta network in the smaller box. The 2 km sea-depth contour is also shown. The filled circles in Iran represent centers of Quaternary volcanism. Geographic features indicated are as follows: AR = Aravalli range, CB = Cambay basin, CF = Chaman fault, CH = Chagai hills, CR = Central Brahui range, GF = Gardez fault, HR = Hazara range, HF = Herat fault, HH = Harboi hills, HK = Hindu Kush region, HM = Himalayas, HS = Hazara-Kashmir syntaxis, K = Kirthar range proper, KF = Kunar fault, KR = Karakorum region, M = Makran region, OF = Ornach-Nal fault, OFZ = Owen fracture zone, P = Pamirs, QTR = Quetta transverse ranges, RK = Rann of Kutch, S = Sulaiman range and SR = Salt range. Several cities are indicated by filled triangles: HRT = Herat, HYD = Hyderabad, KAR = Karachi, KBL = Kabul, LAH = Lahore, NDI = New Delhi, QUE = Quetta, RWP = Rawalpindi. The inset in the lower right hand corner shows the plate tectonic setting of the region.

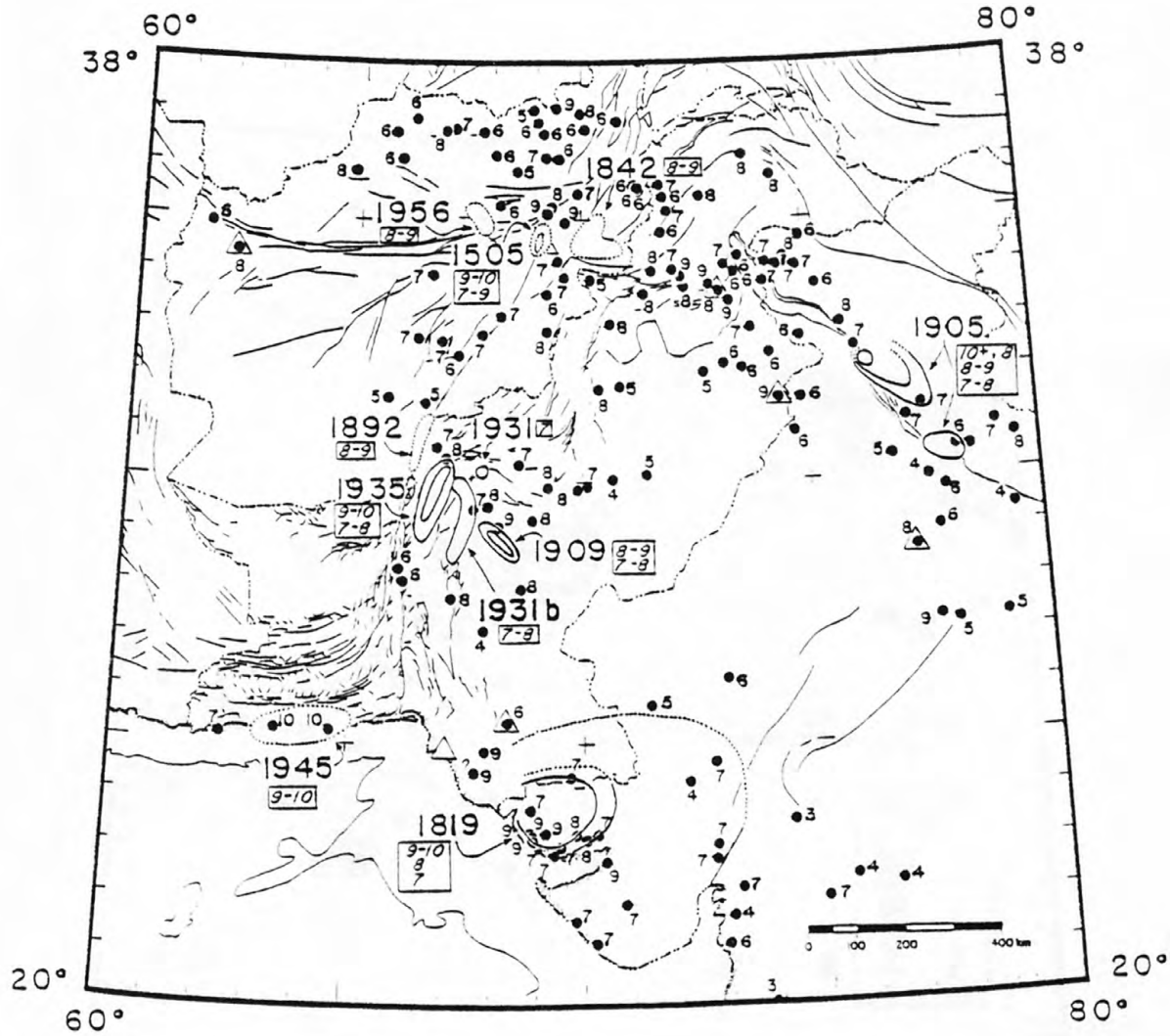

Figure 2. Map of maximum documented intensity (Modified Mercalli Scale) at any given location (Quittmeyer et al., 1979). Data for the time period ~ 25 A.D. to 1972 are shown. Isoseismal lines (dotted where inferred) are plotted for some of the larger events. The year of occurrence for each such large event is indicated. The intensity value associated with a given isoseismal line is indicated in the box near each date. The first value given is for the innermost isoseismal line, etc. Isoseismal lines for the 1905 event are after Middlemiss (1910), those for the 1909 event are after Heron (1911), and those for the 1931, 1931b, and 1935 events are after West (1934, 1935). The open triangles represent the same cities shown in Figure 1.

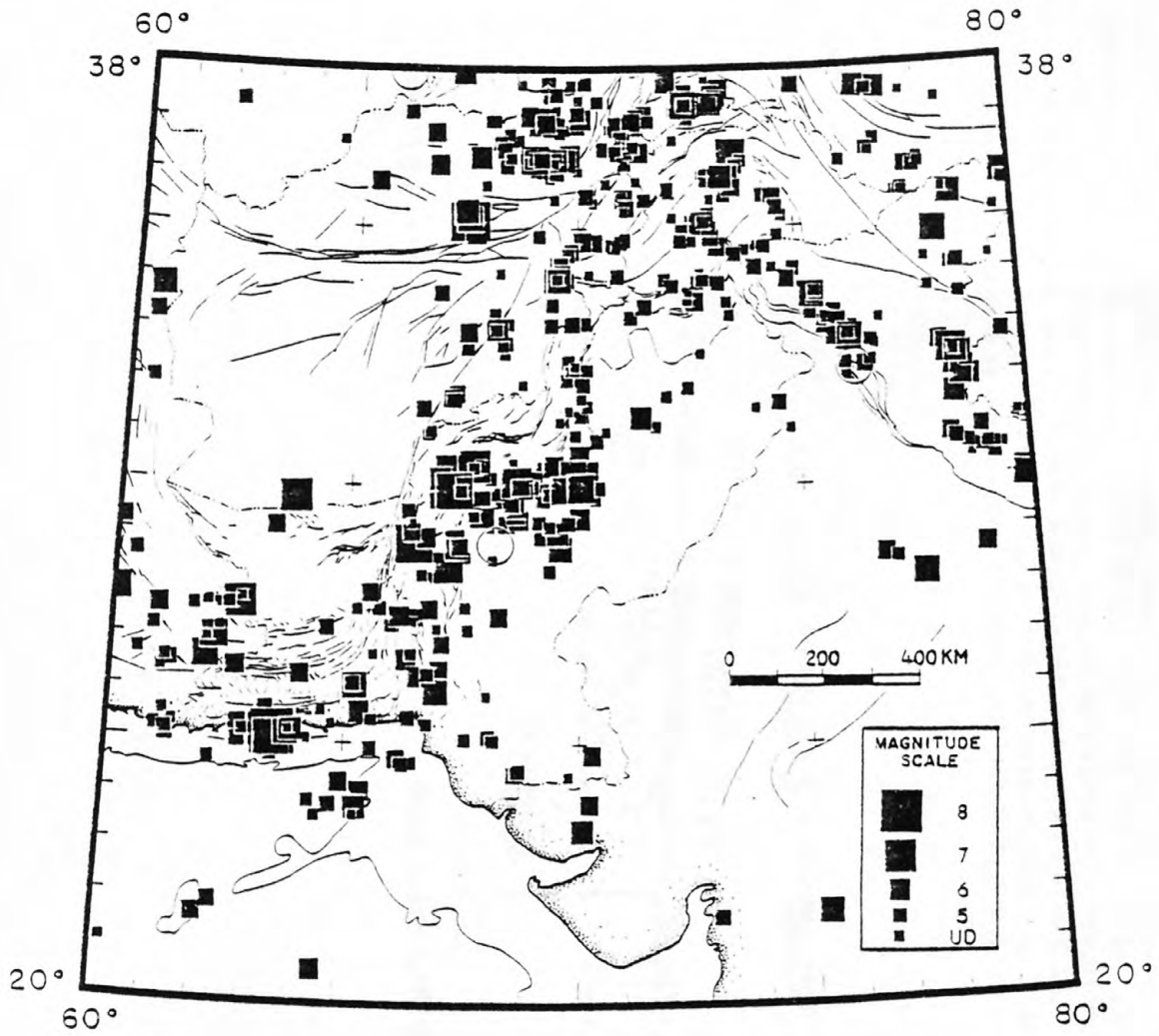

Figure 3. Epicentral map of crustal seismicity (depth h < 85 km) for Pakistan and surrounding regions (compare with Figure 2) from 1914 to 1975. Events from 1914 to 1964 have been relocated. Open circles represent large earthquakes that occurred from 1905 to 1914. UD = Undetermined magnitude. Open circles, events 1905-1914. (From Quittmeyer and Jacob, 1979).

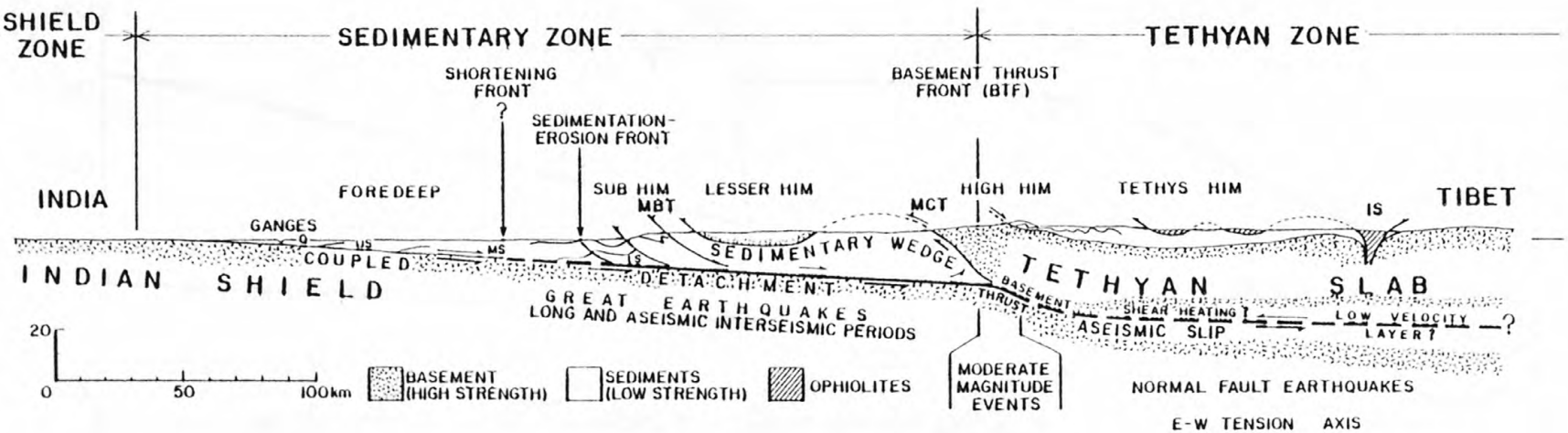

Figure 4. Model (to scale) of the Himalayan continental subduction structure in the central portion of the arc (compare with Figure 5). The progressive stages of the upper surface of the subducting slab are: (1) subaerial in the shield zone, (2) buried below the sedimentary wedge, first as a non-tectonic contact, then as the detachment with great earthquakes, (3) buried below the Tethyan slab, first as the seismically active basement thrust down-dip from the BTF, then as the aseismic but still active contact between basement slabs. The arrows indicate qualitatively the relative velocity in a frame fixed to the Tethyan slab. Q = Quaternary, US, MS, LS = Upper, Middle, Lower Siwalik, MBT = Main Boundary Thrust, MCT = Main Central Thrust, IS = Indus Suture.

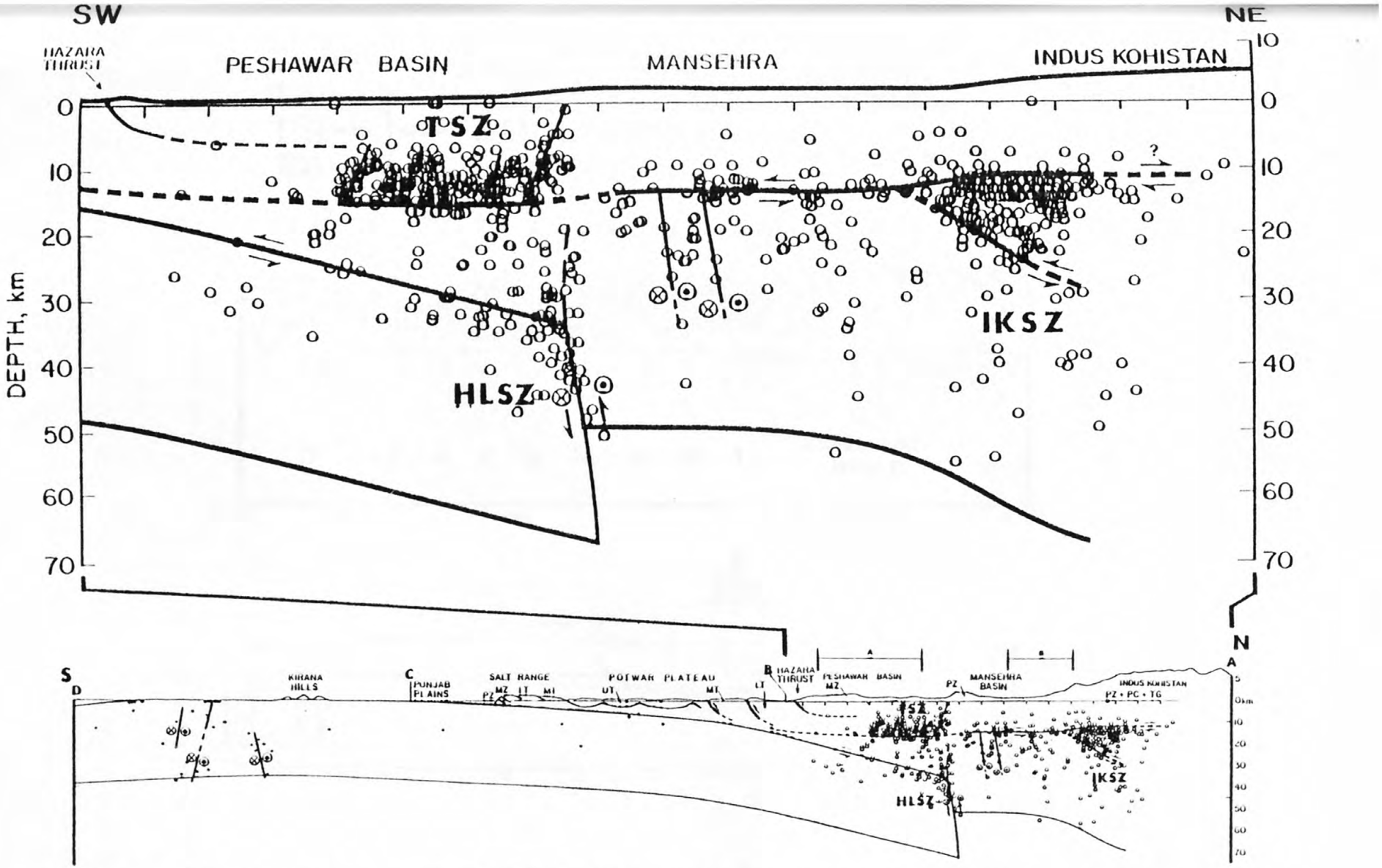

Figure 5. The active tectonic structure in the Hazara arc region as tentatively deduced from the seismicity detected by the Tarbela network. The hypocentral data from a strip along this section is also plotted; the section is located in Figure 3. The sense of movement on the faults in the portion A-B of the section is known from composite fault-plane solutions; ⊗ = motion away from viewer; ⊙ = motion towards viewer; UT, MT, LT = Upper, Middle, Lower Tertiary; MZ = Mesozoic; PZ = Paleozoic; PC = Precambrian; TG = Tertiary granite; HLSZ = Hazara Lower seismic zone; IKSZ = Indus-Kohistan seismic zone; TSZ = Tarbela seismic zone. The Detachment, the quasi-horizontal fault that extends from the base of the Salt range to the IKSZ and beyond, is active even where seismicity is presently absent. On these portions of the Detachment slip may occur either aseismically or by rare large earthquakes (compare with Figure 6). The Moho is arbitrarily drawn at 35 km below the upper surface of the basement.

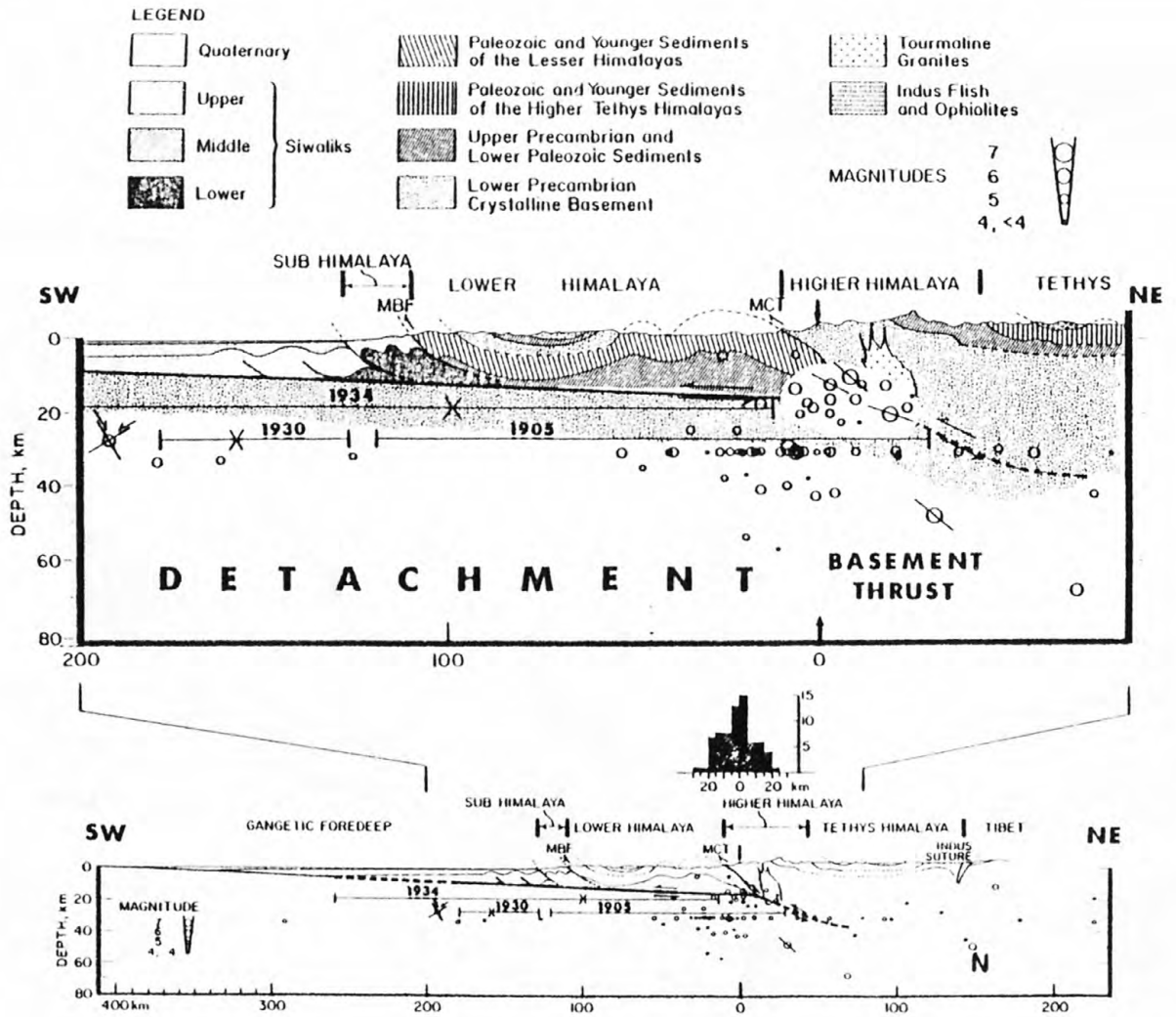

Figure 6. Cross sectional view of seismic data from the central Himalayas. The Detachment and Basement Thrust are shown with respect to regional geology. NOAA hypocenters (1963-1977) from 78°E to 83°E (approximately) are projected along the Himalayan arc onto the section (open circles). The preferred nodal planes for some fault-plane solutions are shown as line segments drawn across the hypocenter symbol. N = marks a normal faulting event with tension axis into and out of the figure. The concentration of earthquakes at 33 km is not real: this depth is arbitrarily assigned to events for which an independent depth determination is not available. The epicenter and extent of intensity VIII (Mercalli I.to X scale) associated with the 1905 Kangra (M = 8), 1930 Dhubri (M = 7.1), and 1934 Bihar (M = 8.3) earthquakes are indicated by crosses and horizontal lines, respectively. Note that the largest earthquakes seem to be associated with the Detachment, while moderate-sized earthquakes in the last decade occur near the transition from the Detachment to the Basement Thrust (histogram). Surface geology is from Gansser (1964, plate II, section A), but below sea-level structures are somewhat modified to fit the model obtained from seismicity.

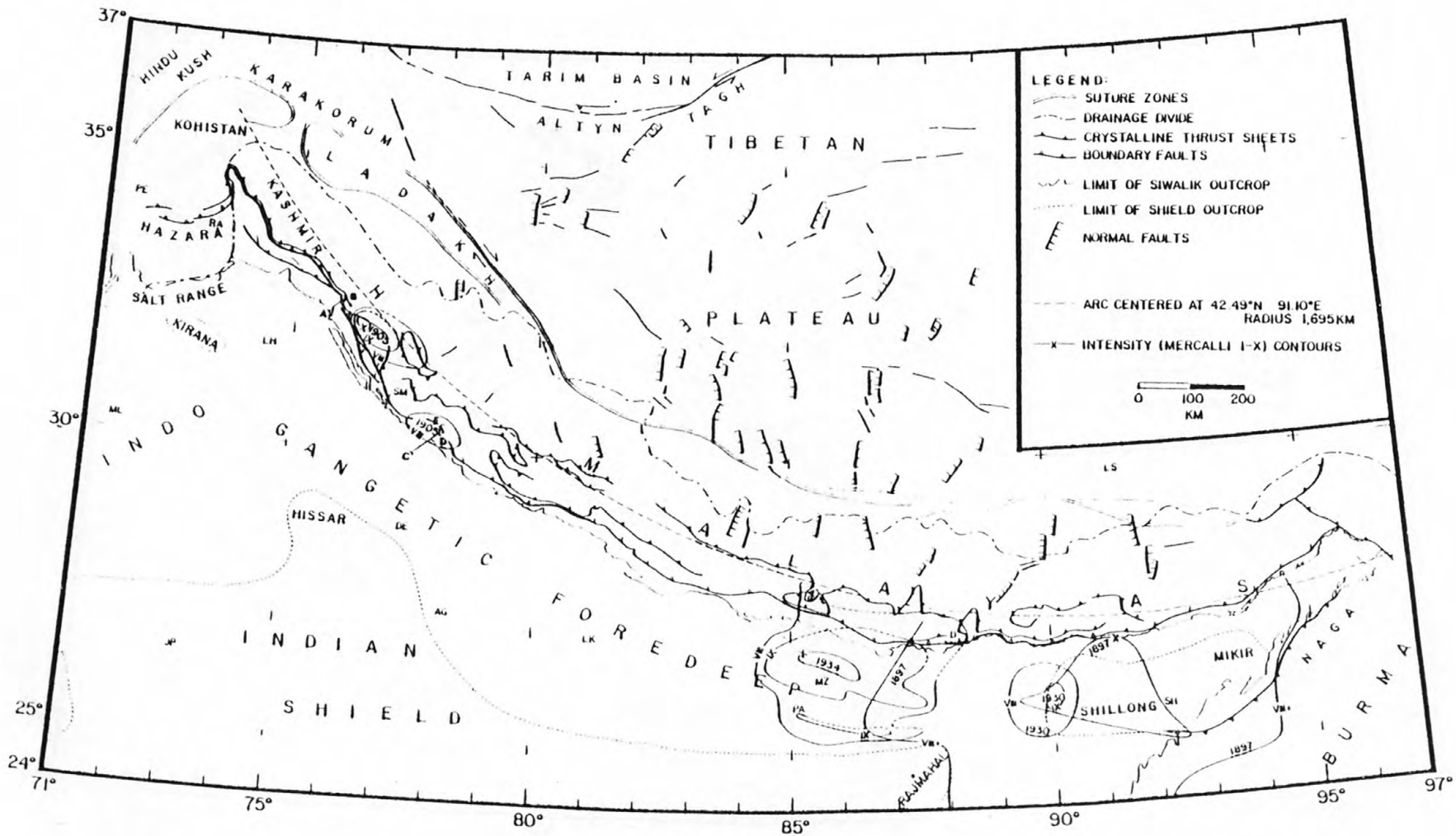

Figure 7. Structural map of the Himalayan arc and Tibet with intensity contours of great earthquakes along the Himalayan front. A-B and C-D-E are leveling lines shown in Figure 11. Note the relation between a small circle fitted to the Himalayan arc and the crystalline thrust sheets. Cities: PE = Peshawar, RA = Rawalpindi, LH = Lahore, ML = Multan, JP = Jokhpur, SM = Simla, DE = Delhi, AG = Agra, LK = Lucknow, PA = Patna, MZ = Muzaffarpur, D = Darjeeling, LS = Lhasa, SH = Shillong.

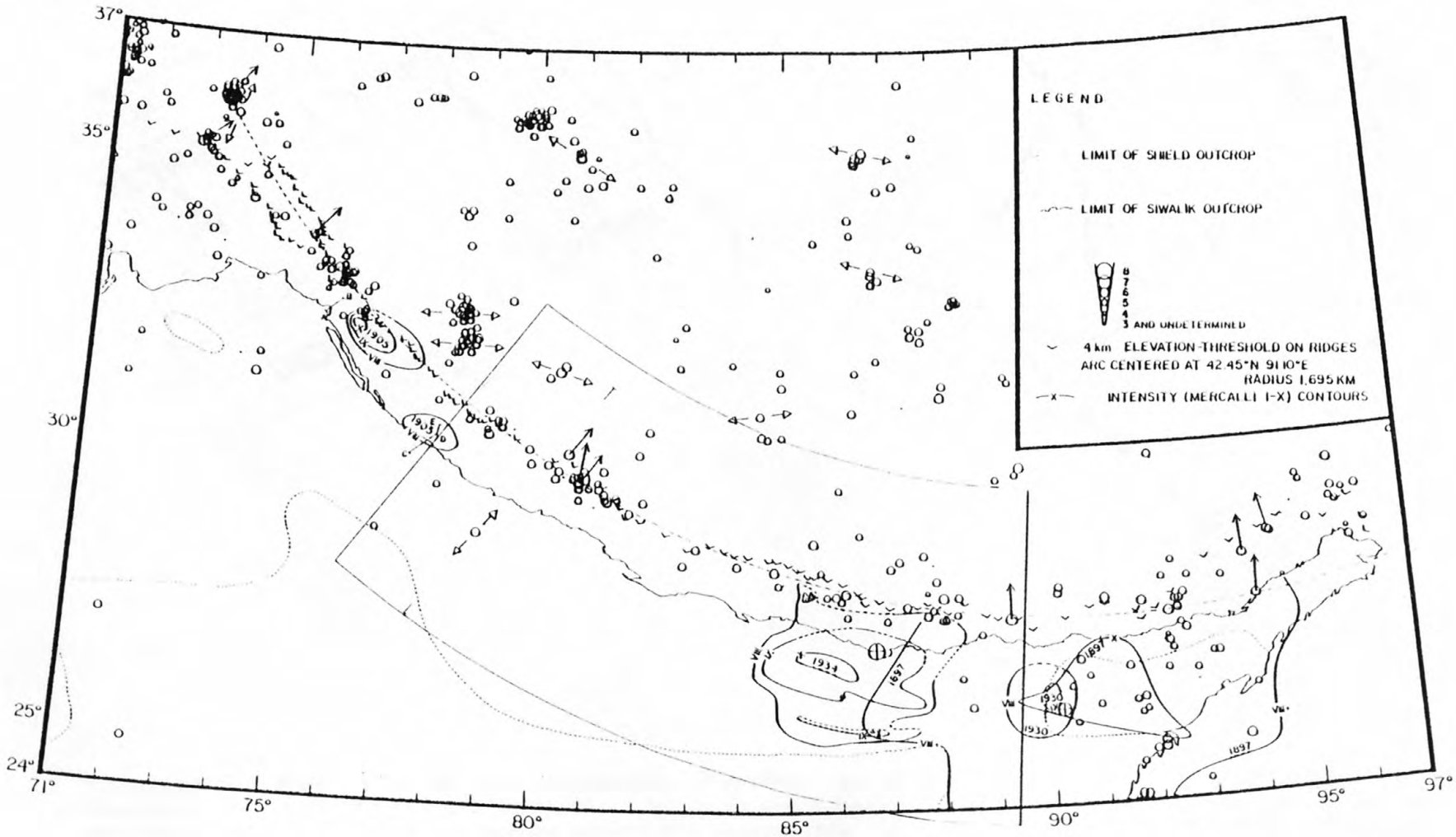

Figure 8. Epicentral map of the Himalaya (NOAA data, 1963-1977), size of circle proportional to magnitude, with intensity contours of Great Himalayan earthquakes. Pairs of arrows = tension axes of normal faulting events. Single arrows = slip direction of thrusting events. Note the agreement between thrusting activity, the threshold of 4 km elevations and a small circle fitted to the Himalayan arc. Data from the boxed section of the arc is plotted in Figure 6. ⊕ = instrumental epicenter of a great Himalayan earthquake.

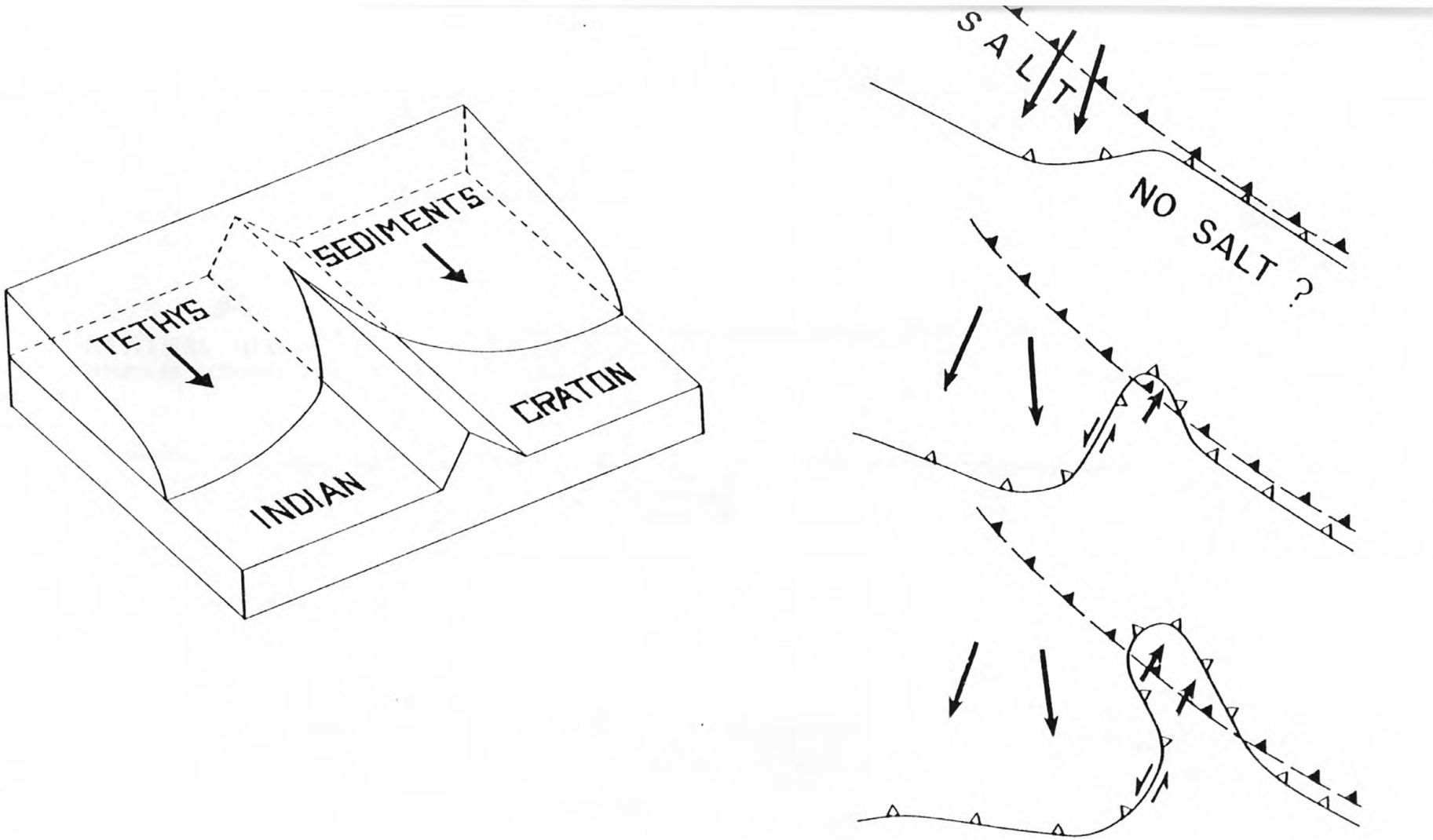

Figure 9. Two sketches of how the northwestern Himalayan syntaxis could have been formed. A) Wadia (1931) suggested that a pre-existing projection or horst on the Indian craton has divided the Himalayan force into two components, molding the structure around the obstruction. B) Our model for the formation of the syntaxis begins with two contrasting portions of the continental shelf of India, one with a thick section of sediments underlain by salt, the second with less sediment and no major effect of salt in the tectonics. Basement thrusting (solid symbol) and the surface expression of faulting (open symbol) remain together where there is no effect of salt, e.g. Basement Thrust Front (BTF) and Main Central Thrust (MCT) in the central Himalaya. Where salt provides a plane of weakness, gravitational force and/or a force generated at a convergent zone further to the northeast pushes the surface features southward from the basement structure, e.g. Hazara thrust and Indus-Kohistan seismic zone (IKSZ) in Pakistan. Figure 10 is a cross sectional view of these same two types of structures, with and without salt.

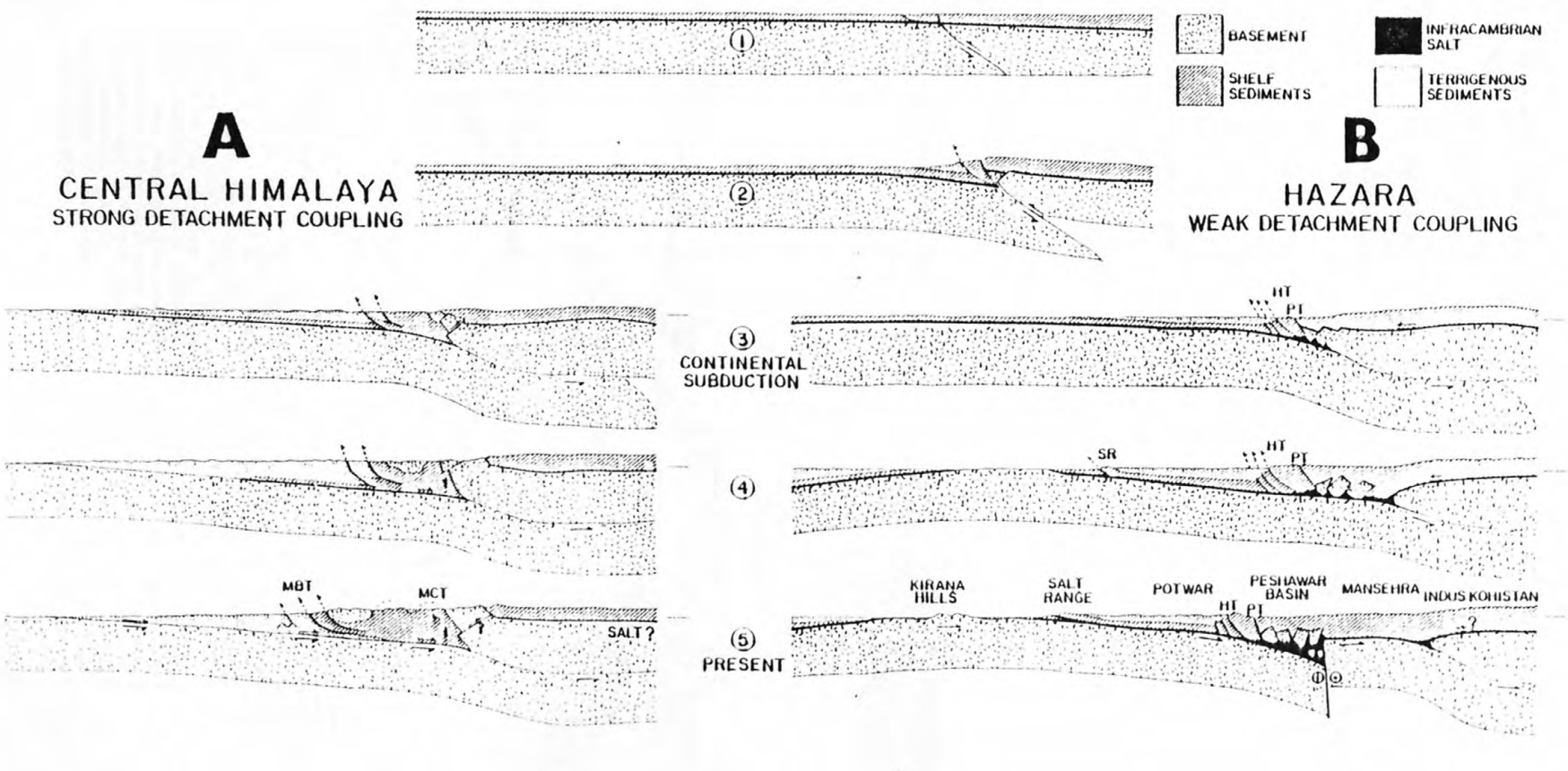

Figure 10 Sequence of tectonic events in the development of the Himalayan continental subduction structure. In this scheme the difference between the Hazara and the central Himalaya sections are primarily a consequence of the coupling at the Detachment. In Hazara the Detachment can develop along the thick Infracambrian evaporite layer and the sediment-basement coupling is weak. In the central Himalaya the Detachment is mostly between the basement and the terrigeneous sediments and the coupling is relatively strong. The distribution of the salt layer in stages 1 and 2 is pertinent to Hazara. In the central Himalaya the Infracambrian salt, if present at all, must have been less extended toward the foreland. Compare stage 5A with Figure 4. HT = Hazara Thrust, PT = Panjal Thrust, MBT = Main Boundary Thrust, MCT = Main Central Thrust.

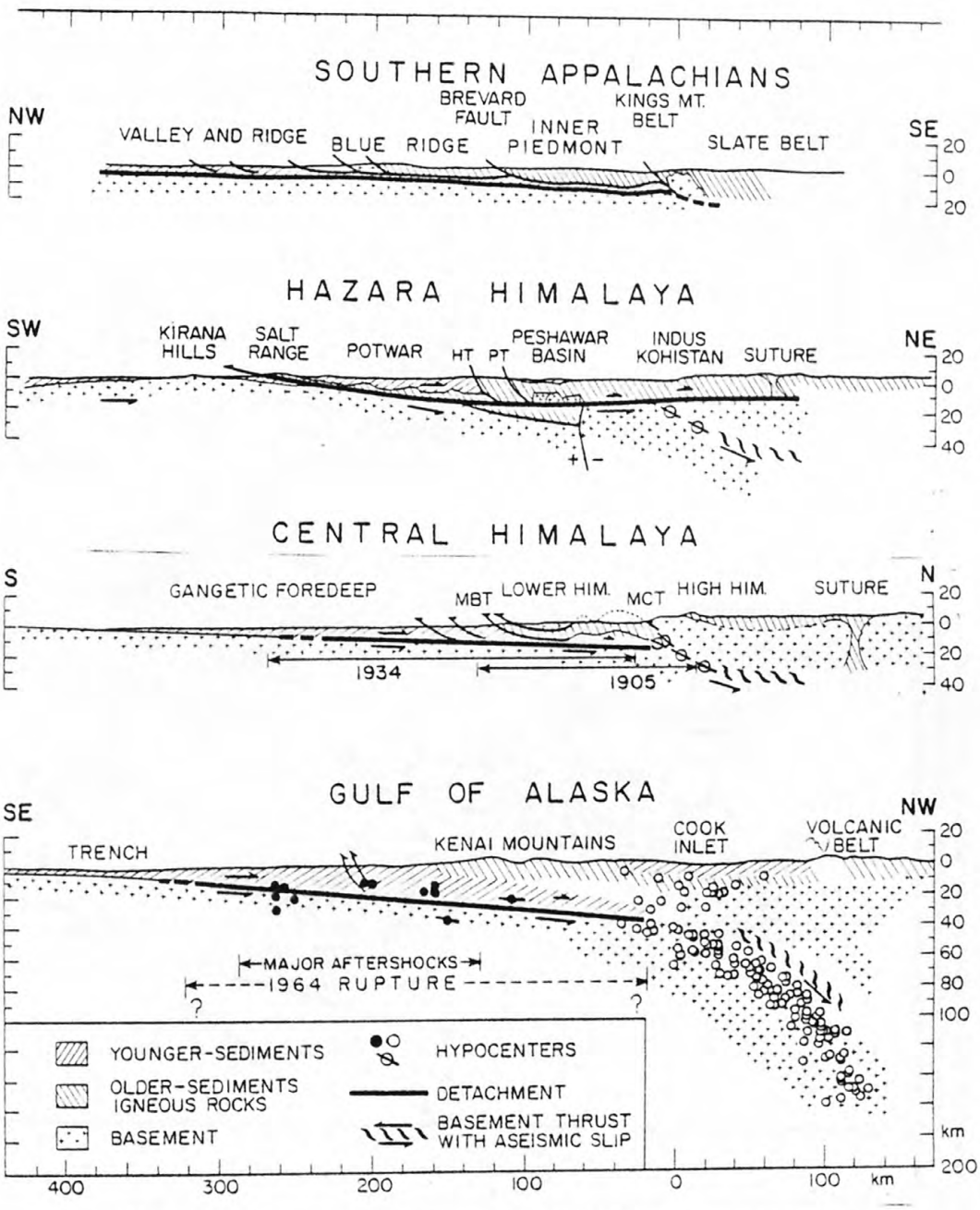

Figure 11. The southern Appalachians, a continental collision structure now inactive, and the active oceanic subduction structure in the Gulf of Alaska are compared to the Himalayan continental subduction structure. The Alaskan section is a superposition of data from the great 1964 earthquake (M_S = 8.4); the filled hypocenters are 1964 aftershocks redrawn from Plafker (1965) with slight changes and hypocentral data from a local network obtained in the interseismic period (April-June, 1972; Lahr et al., 1974). The Southern Appalachian section is deduced from recent deep seismic reflection results (COCORP; from Cook et al., 1979). In the Himalayan section the arrows associated with the great earthquakes (1905, M_S = 8.0 and 1934, M_S = 8.3) indicate the respective extent of intensity $\geq$ VIII which we correlate with the extent of rupture. Note that the great earthquakes are associated with the detachment in both oceanic and continental subduction structures. The four thrust earthquakes in the Himalayan section between the aseismic thrust and the detachment (the bar through the hypocenters indicate the dip of the inferred rupture plane; see Figure 4) indicate the location of the seismically active portion of the thrust. Thrust earthquakes in oceanic subduction structures are similarly located (cf. Isacks and Barazangi, 1977).

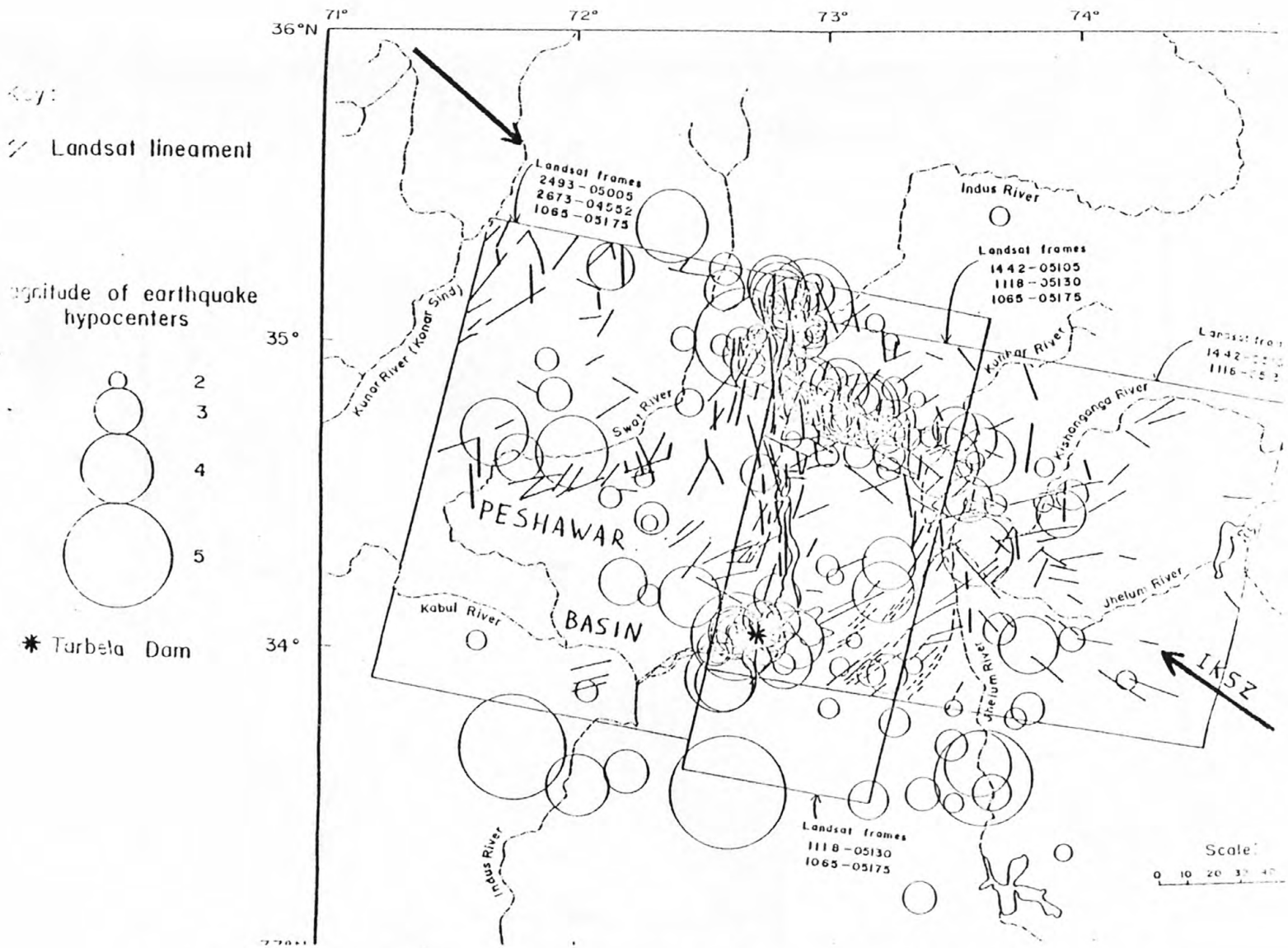

Figure 12. Composite Landsat lineament map superimposed on seismic map of Tarbela network, for hypocentral depths between 12 and 30 km, between August 16, 1973 to August 22, 1976. Diameter of circle is proportional to local magnitude, for events with magnitudes $\geq$ 2.

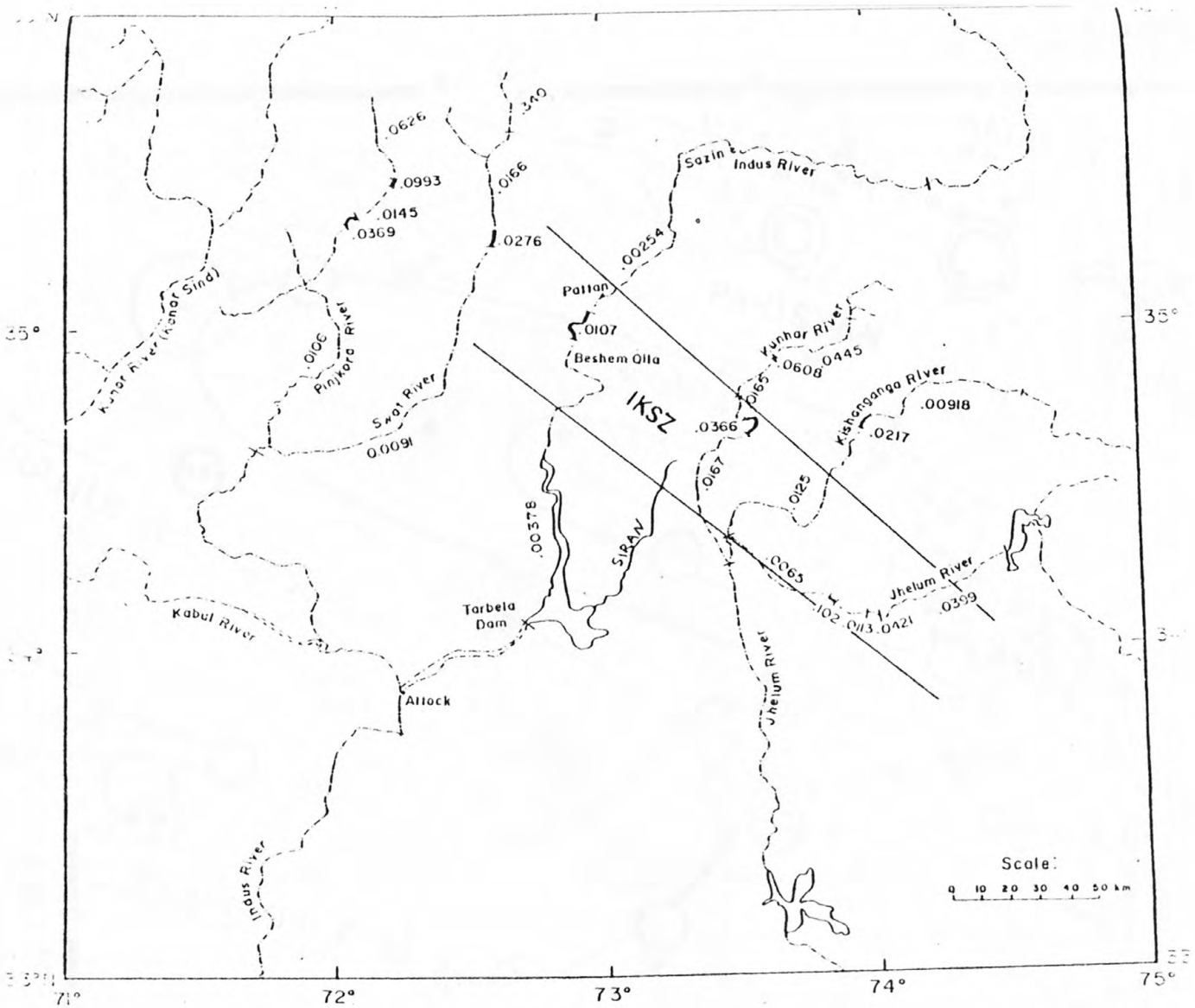

Figure 13. Distribution of knickpoints on major rivers and their relation to the Indus-Kohistan Seismic Zone (IKSZ). The average gradient of a river segment is indicated by the number between thin lines. A knickpoint or segment of increased gradient is shown between double lines.

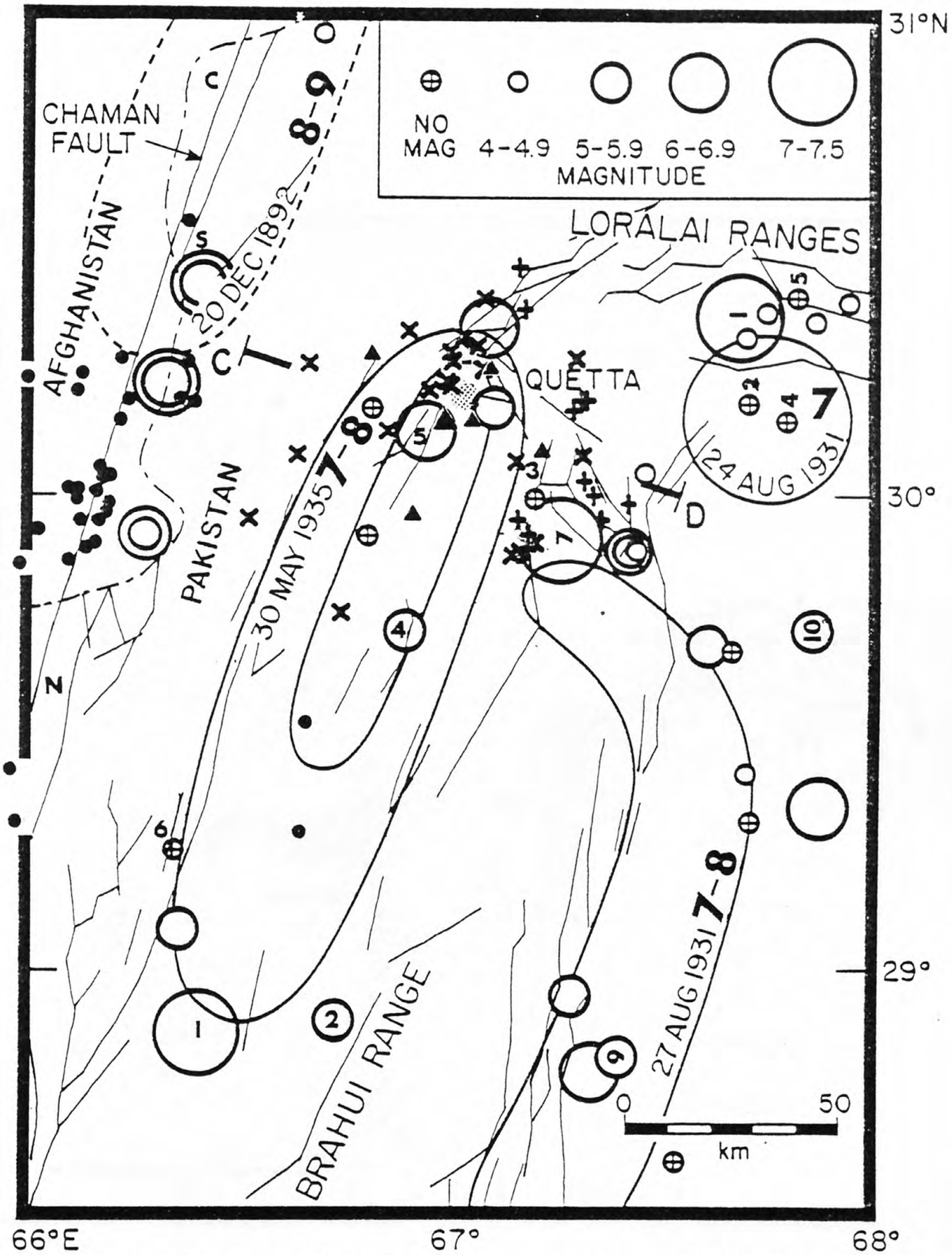

Figure 14. Earthquake epicenters in the Quetta area from 1914 to July 1975 (open circles) and Modified Mercalli isoseismals for the three largest earthquakes in this period as well as the 1892 event (from Quittmeyer and Jacob, 1979). Double circles indicate epicenters for earthquakes occurring after this time period: The 3 October 1975, magnitude Ms = 6.4, Spin Tezha earthquakes; the 13 July 1977, magnitude Ms = 5.5, Kolpur earthquake southeast of Quetta; and the 16 March 1978, magnitude Ms = 5.9, Nushki earthquake. C = town of Chaman; S = Spin Tezha; N = Nushki. Sequences of events are indicated by number: 1935 Quetta = numbers upright, 1913 Mach = numbers facing right (some fall outside the map). Preliminary epicenters from the Quetta network (filled triangles) are indicated by X (hypocentral depth ranges from 0 to 15 km), + (hypocentral depth ranges from 15 to 30 km), and filled circles (hypocentral depth fixed at 15 km). Note the recent (1975) increase of seismicity on the section of the Chaman fault in this figure and the striking

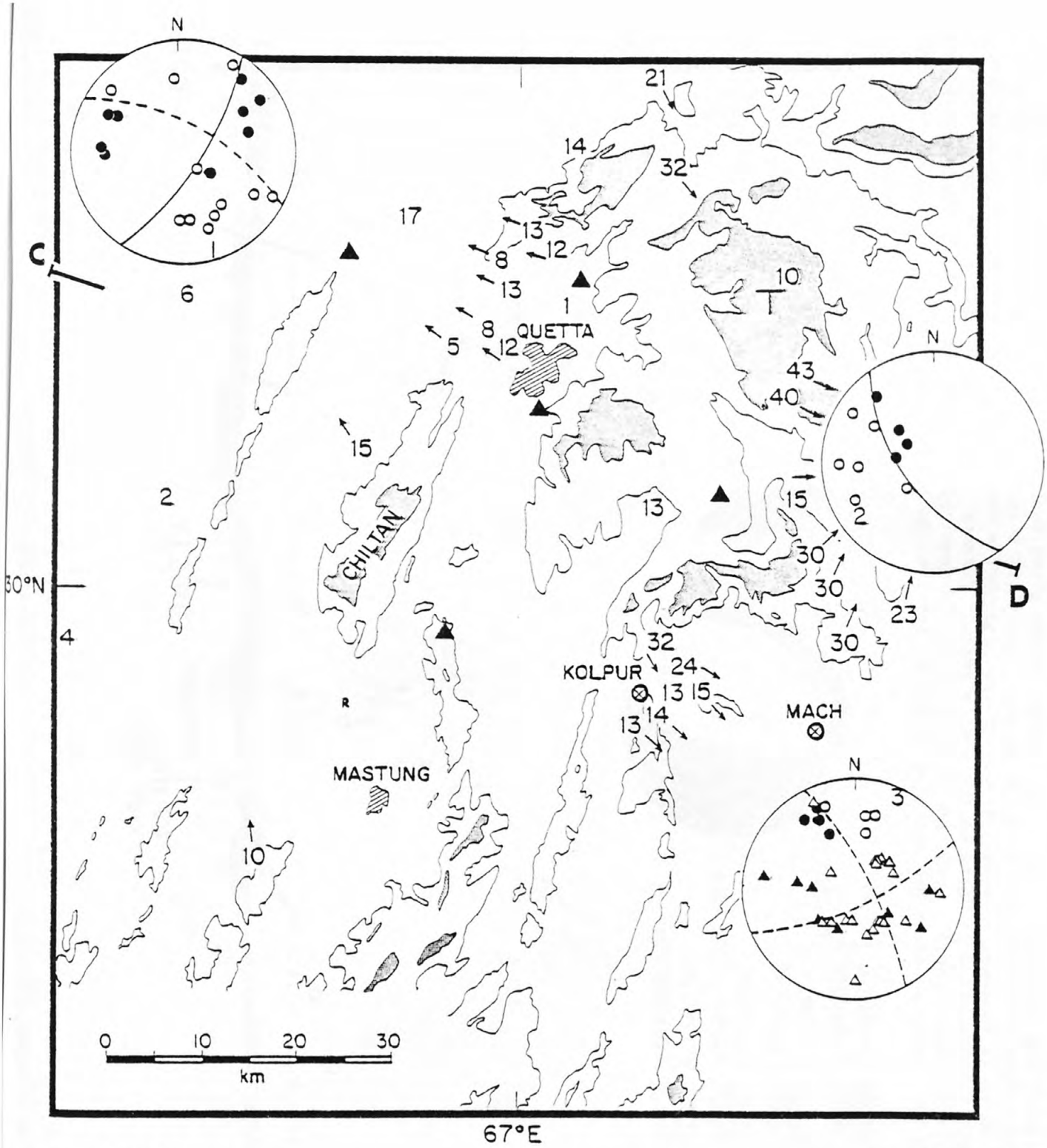

Figure 15. Detailed map of the local activity recorded by the Quetta seismic network (triangles). Events are indicated by a number which gives hypocentral depth in kilometers. Topographic contours at 2000 and 2500 meters are shown with areas above 2500 m shaded. "T" indicates Oligocene to Pleistocene age deposits which have been uplifted. Three composite focal mechanism solutions are shown in upper hemisphere projections; filled circles compressions open circles dilitations. Arrows indicate events which were included in each composite. The number identifying the fault plane solution lies at the position of the axis of maximum compression ("2" is at the position consistent with thrusting). Solution number 3 also includes teleseismic data (triangles) for a large event which occurred before the network began operating (July 13, 1977; see Figure 14). Some geographic features referred to in the text are indicated. Section C-D is shown in Figure 16.

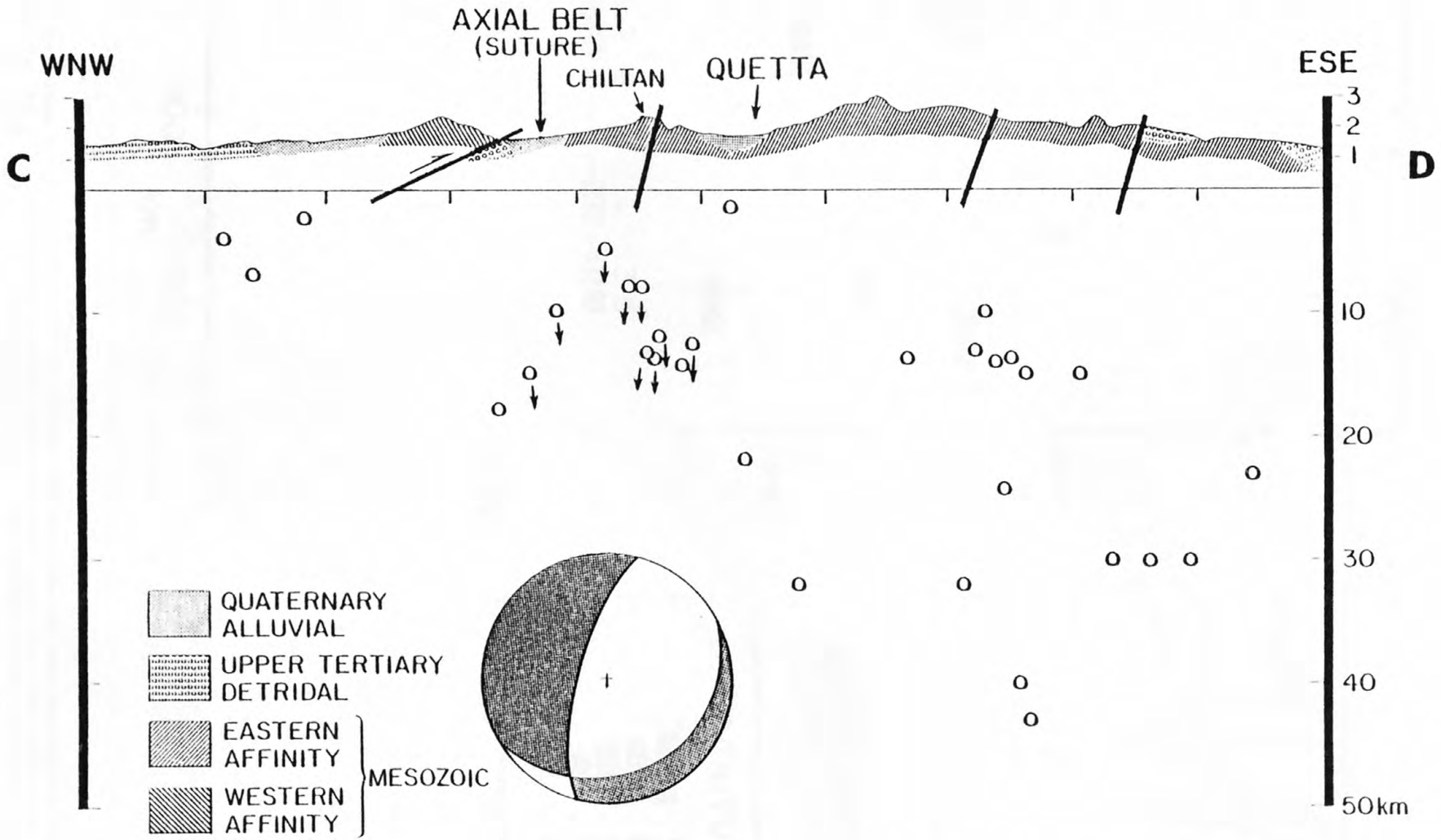

Figure 16. Vertical cross section (C-D in Figure 15) through the Quetta seismic network with main geologic structures (Jones, 1961). Note that upper Tertiary includes the Pleistocene in many cases. Small circles indicate hypocenters determined by the Quetta seismic network. The focal mechanism for events along the fault which is presumed to have ruptured in the 1935 Quetta earthquake is also shown (upper hemisphere, viewed from this side, compressional quadrant shaded). Note the agreement between the Chiltan fault on the east face of Chiltan, and the fault plane as determined by the focal mechanism. Some of the scatter in the seismicity related to this mechanism can be attributed to bending of the fault trace north of the Quetta valley. The shallow dipping fault to the west also appears to be active. The activity in the eastern half of the figure is not oriented well for viewing in this projection.

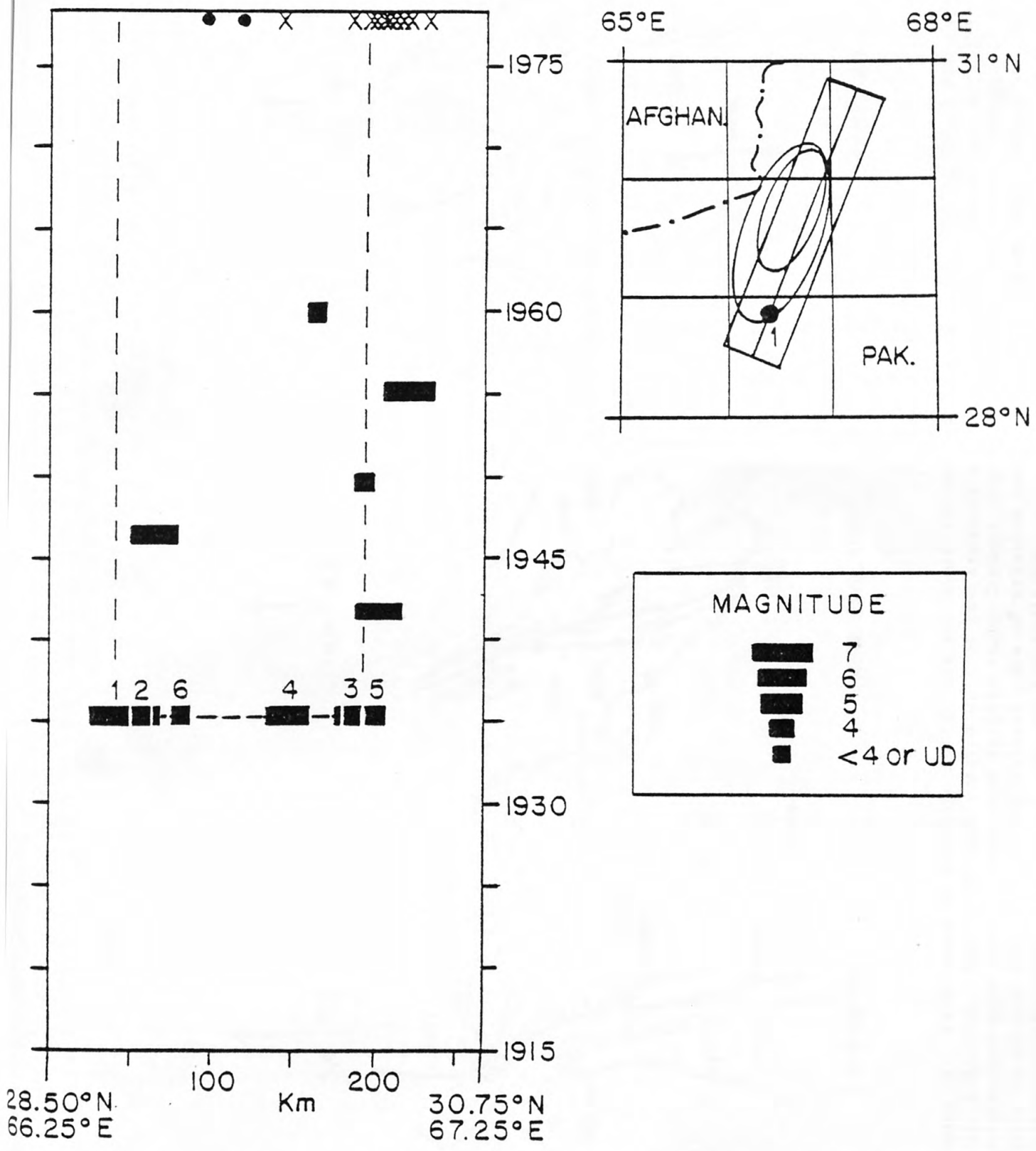

Figure 17. Space-time for the Quetta fault. In the map, the box gives the area sampled; the isoseismals and the epicenter for the 1935 earthquake are shown for reference (see Figure 14). The dashed lines indicate the extent of the aftershock zone. Crosses and dots in 1978 are the epicenters from the network data (see Figure 14). Note that the seismicity after the 1934 earthquake is concentrated near the ends of the rupture associated with this earthquake.

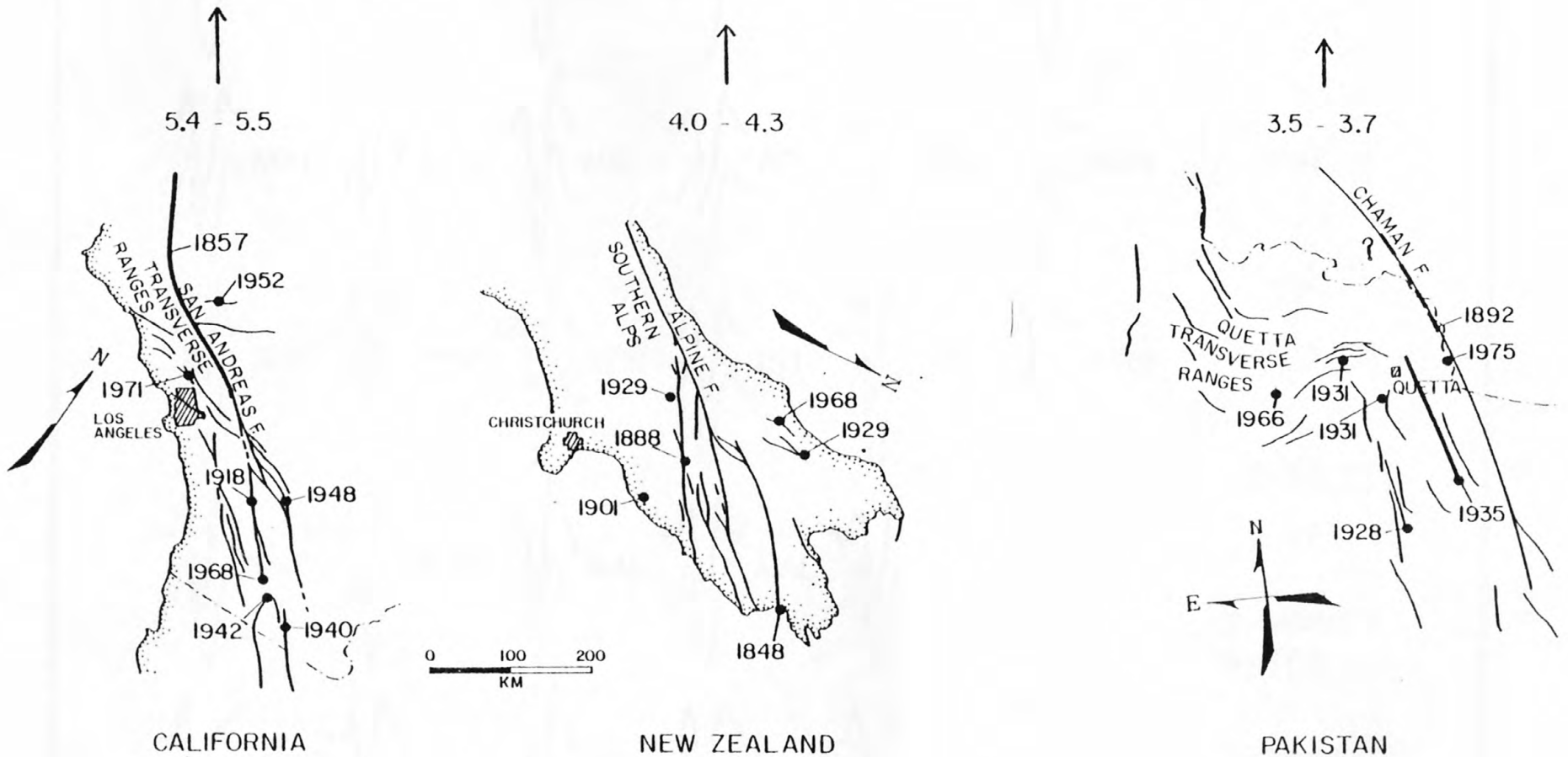

Figure 18. Fault maps of southern California and South Island New Zealand (from Scholz, 1977) and the Quetta area, Pakistan. They have been rotated so that the regional slip vectors (arrows above) are parallel and Pakistan has east and west reversed to give right-lateral strike-slip in all three areas. Length of the slip vector is proportional to the approximate rate of relative motion between major plates (rate given in cm/yr). Dates of earthquakes and zones of rupture are indicated.

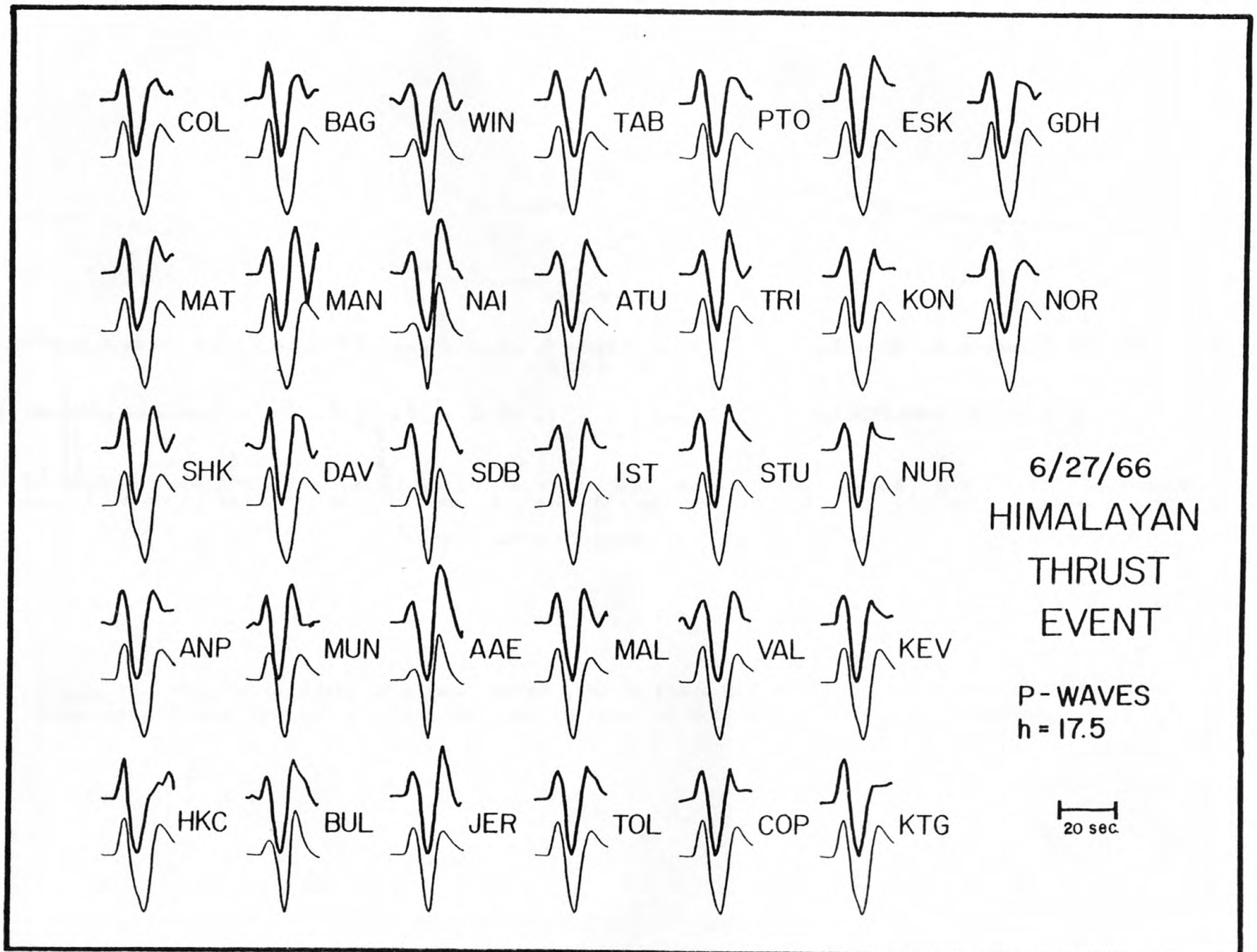

Figure 19. Example of modeling of the body waves of events along the Himalayan front to more precisely determined focal mechanism and hypocentral depth. This event is located at 29.6N and 80.9E in Figure 8.

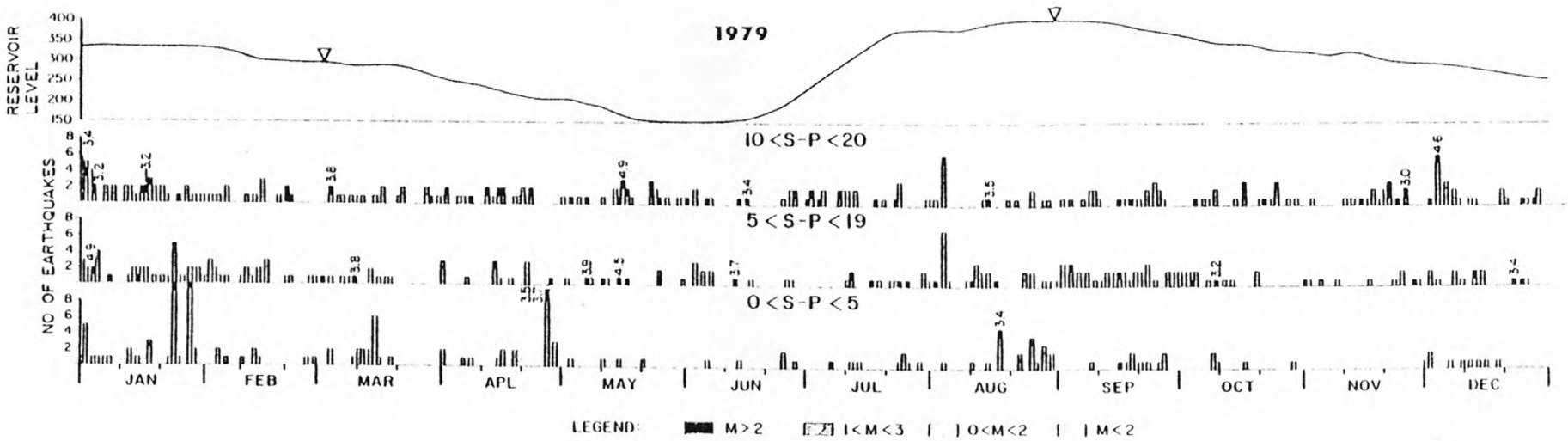

Figure 20. Plot of activity as a function of time in three distance ranges centered on Tarbela Reservoir. There has been a recent decrease in level of activity close to the reservoir.